Final
6/25/01

ACOUSTIC RADIATION PRESSURE-INDUCED FRACTURE OF THE WATER-AIR INTERFACE

BY

NASER HAMZEH DARWISH

B.S., University of Illinois at Urbana-Champaign, 1996

THESIS

Submitted in partial fulfillment of the requirements
for the degree of Master of Science in Nuclear Engineering
in the Graduate College of the
University of Illinois at Urbana-Champaign, 2001

Urbana, Illinois

Red bordered page

ACKNOWLEDGEMENTS

I would like to thank the Nuclear Engineering Department at the University of Illinois for allowing me to perform my research in the Bioacoustics Research Laboratory at Beckman Institute.

I thank my advisor, Dr. William O' Brien, for his guidance, support, and teaching. I also thank everyone in our research group for all their help and support.

My deepest gratitude goes out to my family for being so patient and understanding of my actions.

TABLE OF CONTENTS

LIST OF FIGURES

LIST OF TABLES

CHAPTER 1

INTRODUCTION

Lung hemorrhage has been attributed to ultrasound at diagnostic levels in mice[15][22], rats[14][22], monkeys[16], rabbits[20], and pigs[21]. In a recent study, animal were exposed to pulsed ultrasound at either 2.8-MHz center frequency (1-kHz PRF, 1.42-μs pulse duration) or 5.6-MHz center frequency (1-kHz PRF, 1.17-μs pulse duration) for a duration of 10 seconds[22]. The in situ (at the pleural surface) peak rarefactional pressure levels ranged between 2.5 and 10.5 MPa for mice and between 2.3 and 11.3 MPa for rats[22].

To examine whether lung damage can be extrapolated to human beings, *in vivo* studies using various species must be compared to human beings at the level of lung tissue. The relevance to humans of laboratory-based findings on ultrasound-induced lung damage has not been identified[18]. Mechanical and biological mechanisms of damage can help identify the exact exposures leading to the lung hemorrhage. The purpose of this thesis is to examine the radiation pressure as a possible mechanism of ultrasound-induced lung hemorrhage.

1.1 Thermal Mechanism

A possible mechanism by which damage can be induced is thermal. In an absorbing medium, a sound field produces mechanical energy, which is converted into heat. The increased temperature has the potential to cause irreversible tissue damage[4]. The rate of temperature rise depends on the temporal average intensity, the absorption coefficient of the medium, the cross-sectional area of the beam, the duration of exposure, and the heat transport processes (thermal conductivity and blood flow)[4]. Temperature rise of several degrees Celsius may result in cell damage varying from denaturing of an enzyme to cell death[14]. If an energy other than ultrasound is used to elevate the temperature of a biological system and at the same time produces a biological effect similar to that of ultrasound, then the effect is referred to as thermal[1]. "If the predicted

maximum temperature elevation is less than 1 ^{0}C in a patient, there is no basis for believing that this exposure could lead to an adverse effect arising from thermal mechanism[1]." To observe the mechanical effects, it is necessary to minimize the thermal component by cooling the medium or by lowering the pulse repetition frequency (PRF)[4].

1.2 Nonthermal Mechanisms

Nonthermal effects can occur through either cavitational or noncavitational mechanisms. Noncavitational mechanisms include radiation force or pressure, radiation torque, and acoustic streaming. The development of each of these concepts will be included.

1.2.1 Cavitational Mechanism

The cavitational mechanism is an activity associated with microbubbles (0.1 μm-5.0 μm)[1]. In order for cavitation to cause damage in the lung, it is essential that an isolated gas bubble or nucleation site be available to undergo the bubble growth and implosive collapse[13]. At diagnostic ultrasonic pressures, if these microbubbles exist then they may grow and burst[13]. The violent oscillations and rapid collapse due to high ultrasonic pressures is referred to as inertial cavitation[13]. Bubble collapse at the gas-liquid interface may generate chemically reactive free radicals, extremely high temperatures, and microjets; which could easily damage the air-blood barrier[18]. The lungs must be aerated to produce lung hemorrhage[14]. However, it is inconclusive to say that inertial cavitation mechanism induces lung hemorrhage by ultrasound[13]. Overpressure reduces the negative total pressure during the pulse, and that increases the threshold for inertial cavitation[13]. If overpressure or increased hydrostatic pressures reduces inertial cavitation and if inertial cavitation mechanism applies for the cause of lung hemorrhage, then a reduction in ultrasound-induced lung hemorrhage is expected[13]. On the contrary, overpressure produces more lung hemorrhage by ultrasound than with lower pressures[13].

1.2.2 Noncavitational Mechanism : Mechanical Mechanisms of Second-Order

There are several nonthermal bioeffects caused by ultrasound that are known to occur in the absence of well-defined gas bodies. It is confirmed that three of these effects occur at exposure conditions similar to those of diagnostic ultrasound[18]. These effects cause damage through shearing and stress; they are radiation pressure or force , radiation torque, and microstreaming[14].

1.2.2.1 Radiation Pressure

If viscosity of the liquid is ignored the following expression applies:

$$P_{rad} = PE - KE + C, \quad (1)$$

Where C is a constant, PE is the time-averaged potential energy density (potential energy per unit volume) of the sound field at the target, and KE is the time-averaged kinetic energy density. In a traveling wave $KE=PE$ so P_{rad} is constant and is equal to [4]:

$$P_{rad} = p_0^2/2\rho_0 c^2 \quad (2)$$

Where p_0 is the pressure amplitude, ρ_0 is the density of the medium, and c is the speed of sound.

Radiation pressure can also be represented in terms of the time-averaged acoustic intensity and the speed of sound in the absorbing media[3]. The result is the expression:

$$P_{rad} = I(TA)/c \quad (3)$$

Therefore, radiation pressure is the increase in steady or time-averaged pressure generated by sound[6].

1.2.2.2 Radiation Force

In a sound field, a body may respond as if acted on by a steady force; this is the radiation force acting on it[6]. The radiation force can be calculated by integrating over the surface the effect of the radiation pressure on the surface. Calculation of a radiation force on a body is difficult in most cases, but relatively simple results apply in certain situations. For example, when an ultrasound

beam is directed normally to the plane surface in an open vessel, the ultrasound produces a radiation force equal to:

$$F_{rad} = W/c, \quad (4)$$

W is the acoustic power and c is speed of sound in the media. When an ultrasonic beam impinges on any surface, a radiation force results. If the surface is a perfect reflector, as would be by an air-water interface, the radiation force for normal incidence is twice that of the above equation for $F_{rad.}$ However, if the reflection coefficient is not very large and the body is highly absorbing, F_{rad} can be described by equation 4.

1.2.2.3 Radiation Torque

Radiation torque causes a body exposed to ultrasound to experience angular momentum. When radiation torque acts on a small suspended spherical body, it sets the body into a steady spinning motion. The more non-uniform the field is, the greater the spinning of the object[1].

1.2.2.4 Acoustic Streaming

Similar to radiation torque, by which ultrasound acts on a discrete body to cause its angular displacement, acoustic streaming acts on elements of a homogenous medium to cause a steady circulatory flow[1]. Acoustic streaming is associated with a large scale such as a water tank and an ultrasonic beam. If the scale is on the order of microns, it is then referred to as microstreaming[1].

CHAPTER 2

LINEAR ACOUSTICS

According to linear acoustic theory, if a radiating surface of transducer vibrates sinusoidally in time with frequency *f* and displacement amplitude; then pressure, particle velocity, and particle acceleration must also vary sinusoidally in time with frequency *f* and amplitude proportional the displacement amplitude [1].

2.1 Traveling Plane Wave

The following equations will consider a travelling wave in the positive x direction in a lossless medium for a single frequency function [3]. Starting with the particle displacement for a continuous wave,

$$\xi = \xi_0 Cos(\omega t - kx) \tag{5}$$

Where ξ_0 is the particle displacement amplitude, ω is the angular frequency, k is the wave numberh, x is the direction along which the wave travels, and t is the time.

The particle velocity U(x,t) and acceleration A(x,t) are determined by differentiating the particle displacement $\xi(x,t)$ once or twice with respect to time. To determine acoustic pressure P(x,t), the following equations must be combined: continuity equation , the equation of state ,and the displacement equation[3]. The following equations result from the above discussion[3]:

$$U(x,t) = -\omega\xi_0 Sin(\omega t - kx) = -U_0 Sin(\omega t - kx) \tag{6}$$

$$A(x,t) = -\omega^2\xi_0 Cos(\omega t - kx) = -A_0 Sin(\omega t - kx) \tag{7}$$

$$P(x,t) = -\rho_0 c_0 \xi_0 \omega Sin(\omega t - kx) = -P_0 Sin(\omega t - kx) \tag{8}$$

A travelling wave transports energy. The energy transported by acoustic waves through a fluid medium has potential and kinetic energy. The kinetic energy results from the moving particles

and the potential energy from the compressed fluid [3]. A particle volume given element has a total energy ΔE given by [3]:

$$\Delta E = V_0\rho_0\{U_0^2 + P_0^2/\rho_0^2c_0^2\}/2 \quad (9)$$

Instantaneous energy density is given by:

$$E_I = \rho_0 U_0^2 = U_0 P_0 /c_0 \quad (10)$$

The U_0 and P_0 are amplitude values of particle velocity and acoustic pressure. The instantaneous particle velocity and acoustic pressures are functions of both position and time. However, the instantaneous energy density E_I is not constant throughout the fluid. The time average of E_I gives the energy density E at any point in the fluid [3]

$$E = < E_I >_t = \frac{\int_0^t E_I dt}{t} \quad (11)$$

The time interval is one period T of a harmonic wave. These expressions apply to any acoustic wave. For a plane harmonic wave traveling in the x direction,

$$P_0 = \rho_0 c_0 U_0 \quad (12)$$

If the P_0 and U_0 are the amplitudes of the acoustic pressure and particle velocity,

$$E = P_0 U_0 /2c_0 = P_0^2/2\rho_0c_0^2 = \rho_0c_0U_0^2/2 \quad (13)$$

For other cases such as spherical or cylindrical, or standing waves, the pressure and particle velocity in equation (13) must be the real quantities obtained from the superposition of all waves present[3]. In the more complicated cases, the above pressure and energy equations may not be applicable. However, it is true that $E = P_0 U_0 /2c_0$ is approximately correct for progressive waves at greater distances from the sources[3][1]. A plane wave approximation is applied for the fountain experiment and the calibrations. Therefore, the above equations hold true at the focus of each of the transducers used in this study.

2.2 Stationary Plane Wave

A stationary plane wave exists when a travelling wave in a lossless medium (a medium in which the attenuation coefficient is zero) hits a boundary at a normal surface and is totally reflected. The incident and reflected wave are superimposed to create the stationary wave, characterized by the following equations:

$$P = P_0 \sin(kx)\sin(\omega t) \tag{14}$$

$$U = (P_0/\rho c_0)\cos(kx)\cos(\omega t) \tag{15}$$

Whereas the $P_0 \sin(kx)$and $(P_0/\rho c_0)\cos(kx)$ vary periodically in space and are equal to P_0 and $P_0/\rho c_0$ respectively at the pressure and the velocity amplitude maxima. The k is defined as $2\pi/\lambda$ where λ is the wavelength of the stationary plane wave in the media. Furthermore, the instantaneous intensity I_I is defined as the product of PU, and it varies sinusoidally with frequency. However temporal average intensity I(TA) is zero everywhere for a stationary plane wave[1].

2.3 Standing Wave

If a traveling wave impinges normally at an imperfect reflector and a reflective wave whose amplitude less than that of the incident wave is generated, then the following equation applies:

$$P=A_0 \sin(\omega t - kx) + B_0 \sin(\omega t + kx). \tag{16}$$

The above equation describes a traveling wave representing a pressure amplitude of A_0 going in the positive x direction. A second traveling wave of amplitude B_0 traveling in the opposite direction is also superimposed. The wave of pressure amplitude A_0 represents the incident wave and that of B_0 denotes the pressure wave amplitude for the reflected wave. Thus, these two waves represent the field of the ultrasound[3].

CHAPTER 3

GOVERNING ACOUSTIC PARAMETERS

It is necessary to select a few important indicators of the bio-effect potential for a device. Indicators are quantities such as the acoustic particle displacement, velocity, acceleration, energy, total acoustic power, energy densities, and intensities. Various intensity parameters along with radiation pressure will be considered for quantification of the bio-effect potential of ultrasound. Specifically, the goal of this thesis is to assess radiation pressure as a possible mechanism of ultrasound-induced lung hemorrhage.

3.1 Power and Intensity Parameters

The development of pulse intensity integral (PII) is essential before introducing the intensity parameters. Pulse duration *(PD)* is the time during which the intensity should be averaged. Pulse duration is 1.25 times the interval between the time when the time integral of the instantaneous acoustic pressure squared reaches 10% and 90% of its final value, the final value being the pulse-pressure-squared integral (P_I). If P_I has been determined, *PD* can be calculated from[4]

$$PD=1.25(t_2-t_1) \tag{17}$$

Where t_1 and t_2 are given by:

$$\int_0^{t_1} P^2 dt = 0.1P_I \tag{18}$$

$$\int_0^{t_2} P^2 dt = 0.9P_I \tag{19}$$

The pulse intensity integral is denoted by *PII*, and is defined as the energy fluence per pulse[2]. *PII* is the basis of the ultrasound system used to find the transducer's focus. *PII* is the time integral of the instantaneous intensity in the pulse, integrated over the whole pulse. *PII* is determined from pulse-pressure-squared integral using [2],[5],

$$PII = \frac{\int_0^t [p(t)]^2 dt}{\rho_0 c_0} \tag{20}$$

$$PII = \frac{I(SPTA)}{PD} = \frac{p_0^{\ 2}}{2\rho_0 c_0 PD} \tag{21}$$

Time average acoustic power output (W) is an exposure parameter to characterize a field generated by a device such as a transducer. It is equal to the integral of the time-averaged intensity I(TA) over the surface traversed by the entire beam[3].

To assess biological effects, the dose of ultrasound must be known. Dose is the quantity of energy absorbed per unit mass of absorbing medium [9]. Closely related to energy absorption throughout the medium is the point-by-point variation of intensity in the medium [1]. Intensity is a very useful parameter that measures the acoustic power flowing at normal incidence to a unit area[3]. The instantaneous intensity I_I is the dot product of P and U. The instantaneous rate at which work is done per unit area by one element of fluid on an adjacent element is PU. Instantaneous intensity I_I for an acoustic wave is

$$I_I = P_0^{\ 2} / \rho_0 c_0 \tag{22}$$

When the intensity of a continuous wave is considered, a time-average of the instantaneous rate is taken.

$$I(TA) = < PU >_t = \frac{\int_0^t PU \quad dt}{t} \tag{23}$$

The integration is taken over a time corresponding to the period of one complete cycle.

The pressure P varies sinusoidally in time and the temporal average intensity is obtained by averaging I_I and is given by

$$I(TA) = P_0^2/2\rho_0 c_0 \quad (24)$$

Time average intensity exists at a spatial peak [4]. This spatial-peak temporal-average intensity is symbolized by *I(SPTA)*. The time-average is taken over an integral number of acoustic repetition periods *(PRP)*. Pulse repetition frequency (PRF) is the number of identical acoustic pulses per second [4]. *PRF* is determined directly by the rate of arrival of identical pulses at the hydrophone. Measurements of most of the above parameters do not refer to a particular waveform, but different waveforms are measured due to the moving hydrophone to any point in the ultrasonic field. Each waveform would have its own set of values to describe the local field. As the transducer emits pulses, it causes large fluctuations of intensity in the region through which the pulses move. Each pulse consists of multiple cycles that produce intensity variations within the pulse itself. The maximum intensity is designated temporal peak[*I(TP)]*, the intensity averaged over the duration of a single pulse is designated pulse average[*I(PA)]*, and the intensity averaged over the longer interval of the *PRP* is designated temporal average[*I(TA]) [4][1]*. For a given pulse sequence, *I(TP)* has the highest value, followed by *I(PA)*, and finally by *I(TA)*. The *I(TA)* is related to the *I(PA)* by the duty factor *(DF)[1]*,

$$I(TA) = DF \times I(PA) \quad (25)$$

Also I(TA) is related to I(PA) by the pulse duration*(PD)* and pulse repetition frequency*(PRF)*,

$$I(TA) = PD \times PRF \times I(PA) \quad (26)$$

For identical pulses,

$$I(TA) = PII \times PRF \quad (27)$$

Therefore,

$$PII = PD \times I(PA) \quad (28)$$

For temporal-average intensity, the time average is taken over an integral number of cycles of the waveform. For continuous waveforms time averaging is usually employed with an intensity specification of *I(SATA)* or *I(SPTA)*. *I(PA)* are not applicable for continuous wave (CW) ultrasound[1],[4].

Intensity exists at spatial peaks. *I(SPTP)* is spatial peak, temporal peak intensity. *I(SPPA)* is spatial peak , pulse average intensity. *I(SPTA)* is spatial peak, temporal average intensity. The designation *SP* refers to the maximum intensity in a plane perpendicular to the beam axis at a particular distance from the transducer. More commonly, however, it denotes the maximum intensity throughout the ultrasonic field, which usually occurs along the beam axis[1],[4].

Spatial averaging *(SA)* over the cross-sectional area of the beam of one of the temporal intensities is also specified. A cutoff point of 0.25 times the intensity at the spatial peak ,*I(SP),* has been established to limit the area over which the intensity is averaged. *I(SATP)* is spatial average, temporal peak intensity. *I(SAPA)* is spatial average, pulse average intensity. *I(SATA)* is spatial average, temporal average intensity. *I(SATA)*is the spatial average of the time-average intensity over the effective cross sectional area A_x of the beam at a given distance from the source. A_x is defined as the area in which the intensity exceeds 0.25 times the greatest intensity which occurs at the distance x [1][4].

Other intensity descriptors have been used to specify the ultrasonic field. The instantaneous peak intensity (I_p) is the maximum intensity with respect to space and time and is the same as *I(SPTP).* The term maximum intensity (I_m) refers to the time-average intensity over the largest half-cycle in the pulse at the spatial peak. For a perfect sine wave I_m equals *I(SPPA).* For pulsed ultrasound, *I(SPTP)* is greater than I_m, which is greater than *I(SPPA*). Cycle-averaged intensity is an alternative for *I(SPPA).* The symbol I_t denotes the *I(SATA)* at the transducer, which has been

spatially averaged over the area of the radiating surface. It is equal to the acoustic power divided by area of the transducer. The intensity of a continuous-wave usually refers to a *I(TA)*[4].

3.2 Nonlinear Acoustics

The basic differential equations of acoustics are nonlinear. The sound fields are described by linear theory only at low amplitudes. Therefore, the field has characteristics that cannot be described by linear theory alone. The mean pressure at a point may be raised or lowered, steady forces may act on objects in the field, particles may be suspended in the fluid and set into rotary motion, steady circulatory flow may be set up in the fluid, and harmonics may play a role[1]. As harmonics are generated, the waveform becomes distorted and attenuation becomes intensity- dependent[1]. Furthermore, at exposures where non-linear distortion occurs, both the beam width and the absorption parameter become functions of the intensity. Radiation pressure should increase because of non-linear absorption. Higher frequency harmonics are more readily absorbed in the medium and thus facilitate energy transfer from the ultrasound waves into the medium[1].

CHAPTER 4

EXPERIMENTAL PROCEDURES

4.1 Characterization Procedure

Characterization is a technique for determining the spatial and temporal transmit-receive field distribution of spherically focused high frequency transducers[12]. Tungsten wire with a diameter of 100μm is used as a pulse-echo target. From this technique, the following parameters are determined for the transducer: center frequency, bandwidth, fractional bandwidth, pulse duration, beamwidth, focal length, and depth of focus. The characterization or wire technique is explained fully in reference[12]. Two transducers called FT#1 and FT#2 were characterized by the wire technique.

4.2 Fountain Effect Experimental Procedure

Experimental work is set up using FT#1 and FT#2 transducers. The experiment is carried out separately for each transducer. A diagram of the setup is illustrated in figure 4.1.The purpose of the experiment is to find the threshold voltage required to break the water-air interface, and the corresponding distance at which the breakage occurs.

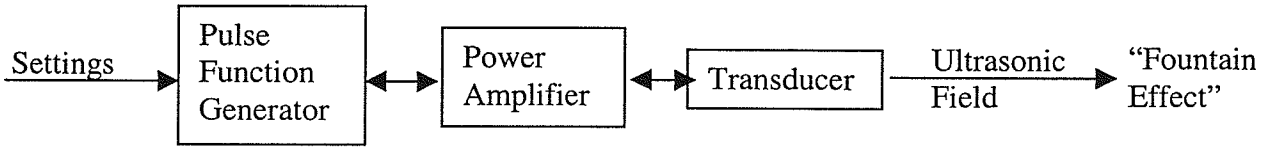

Figure 4.1 Block diagram of the fountain effect experimental setup

Each transducer is placed in a holder at the bottom of a tank that is filled with degassed (distilled water, 22 °C) water. The degassed water is used to eliminate any effects of cavitation. The transducer is remained stationary with its surface facing the top of the tank or the positive z-axis. The transducer is connected to the output of a power amplifier(A-500 RF, ENI, Rochester, NY) and

the input of the power amplifier is connected to the output of a pulse function generator(HP 8116A, Boblingen, Germany). The pulse function generator can produce continuous and pulsed waves. The pulse function generator operates under internal burst mode for pulsed waves and operates under sinusoidal continuous wave for continuous waves. The pulse function generator also controls the frequency and voltage parameter used to drive the power amplifier. The tank is filled with degassed water to a level of several centimeters above the distance at which the maximum PII occurs from the transducer surface. The maximum PII and the distance at which the maximum PII occurs are obtained from the calibration which will be discussed in the next section. A voltage is applied until the water-air interface is broken at the initial 16cm distance. Detail of the fracture is described in the chapter 5 and the pictures of the breakage in the surface are shown in figures 5.11 to 5.13. Once the surface is broken, the function generator is disabled in order to observe the voltage and measure the corresponding distance. Approximately half of a cup of water is taken out at a time and the procedure is repeated. The voltage that is required to break the water-air interface is recorded at each distance away from the transducer surface. The experiment is independently done for each transducer's first and third harmonic frequency. For the pulsed wave experiment, the pulse repetition period (PRP) is varied, but the number of cycles remains constant at 80 cycles. A long pulse can be estimated to be similar to a continuous wave at 80 cycles, and this is the number of cycles used in the calibration. The experiment is repeated at pulsed acoustic wave at PRP of 30μs, 60μs, and 90μs at each transducer's first harmonic frequency. The reason the above values of PRP are used is that hardly any effect is observed at PRP greater than 90μs. The voltage amplitudes are converted to pressure amplitudes by calibrating the transducer at each voltage.

4.3 Calibration Procedure

The power amplifier (A-500 RF, ENI, Rochester, NY) is used to generate driving signal to the transducer by amplifying the signal created by the pulse function generator(HP 8116A, Boblingen, Germany). The function generator is set under internal burst mode or pulsed mode and

set at 80 cycles and PRP of 200 μs. The PVDF hydrophone (GEC-Marconi, Ltd., Essex, England) is the sensor of the ultrasound field. It measures the ultrasound field generated by a transducer. The output measurements from the hydrophone goes into the LeCroy Oscilloscope (LeCroy Model 9354TM, Chestnut Ridge, NY). The Daedal Position Control System(DSPC) (Daedal Inc., Harrison City, PA) moves the hydrophone around the ultrasonic field, and gets the sampled data from the oscilloscope. A diagram of the setup is illustrated in figure 4.2.

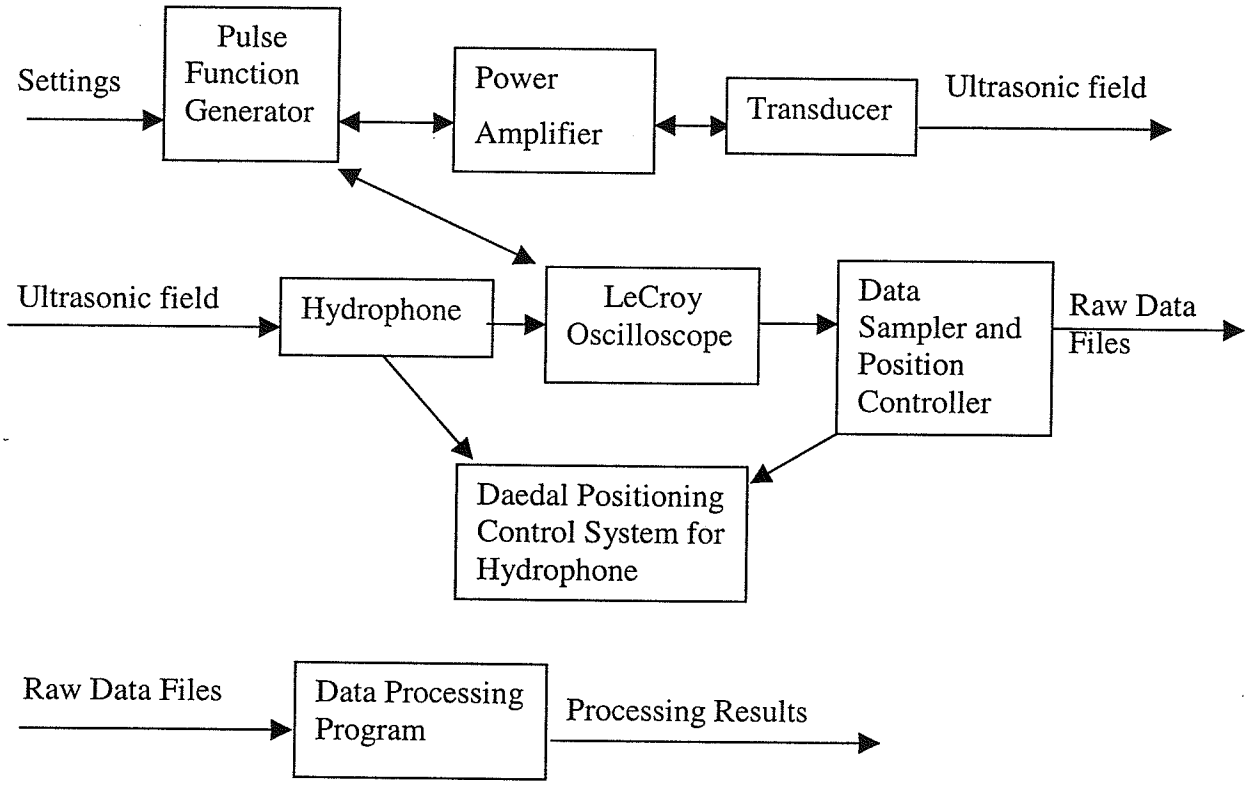

Figure 4.2 Block diagram of the calibration setup

To determine the acoustic pressure values at the focus of the transducer, the transducer's beam axis must be found first. The definition of a beam axis is " a straight line joining points of maximum pulse intensity integral measured at several different distances in the far field."[5] An automated method is used to determine the beam axis which includes a positioning system, a power amplifier , an oscilloscope, a hydrophone ,a transducer, a tank with degassed water, and a computer(Dell Optiplex Gx1p, Pentium-II). The Dell computer contains the C++(Microsoft Visual

C++ 5.0) software for controlling the positioning system and the oscilloscope. As soon as the data collection is completed, the data are transferred to a workstation (SUN UltraSparc) for analysis.

The data acquisition process consists of the manual setup, determination of the beam axis by finding the maximum *PII* along the distance from the transducer, and the collection of RF waveforms along the beam axis.

During the manual setup, the beam axis is determined by finding the pressure field's maximum signal on the oscilloscope. The source transducer is manually placed in a water tank(degassed water, 22 ^{o}C) where the beam axis is parallel to the y-axis. Axis 1, 2, and 3 are the y, x, and z axis respectively and are indicated in figure 4.3. The hydrophone is connected to the computer controlled micropositioning system (Daedal). Each of the three orthogonal axes has a linear accuracy of 2 μm. The hydrophone is moved to a position of 2 mm in the negative axis 2 and axis 3 directions and 15 mm in the positive axis 1 directions. The hydrophone is moved along axis 2 and 3 to scan the axis where *PII* is maximized within the axis 2-3 plane. The maximum *PII* is found between the transducer and the geometric focus as the hydrophone is moved in the positive axis 1 direction in the axis 2-3 plane. At the origin of the scan, the hydrophone is positioned at $-2mm$ in both the axis 2 and axis 3 directions, and $+15mm$ in the axis 1 direction. For determination of the beam axis, the maximum *PII* is determined at 10 axial positions, 5 for axis 2 and 5 for axis 3. The collection of maximum *PII* occurs in increments of 125 μm along axis 1 for a distance of 30 mm in the axis 1 direction. The hydrophone moves from the origin in a 125 μm increments a distance of 4 *mm* in the axis 2 direction searching for the signal with the maximum *PII*, and then the hydrophone returns to the origin. The position corresponding to the maximum *PII* is stored for later purposes. The same method applies for axis 3 direction. There is a position that corresponds to maximum *PII* for axis 1 and another position that corresponds for axis 2. The search for the maximum *PII* is repeated at 5 equally divided intervals along axis 1. From the maximum *PII* at each coordinate along axis 1 , a best fit line can be drawn which corresponds to the beam axis of the transducer. The

hydrophone then moves back to (0,x,y) after the beam axis has been calculated. The hydrophone moves in 125μm increments along the beam axis and collects RF waveforms at a sampling rate of 500 Ms/s. Finally, the waveforms are transferred to Sun UltraSparc workstation where the data is analyzed using Matlab (The Mathworks, Natick, MA).

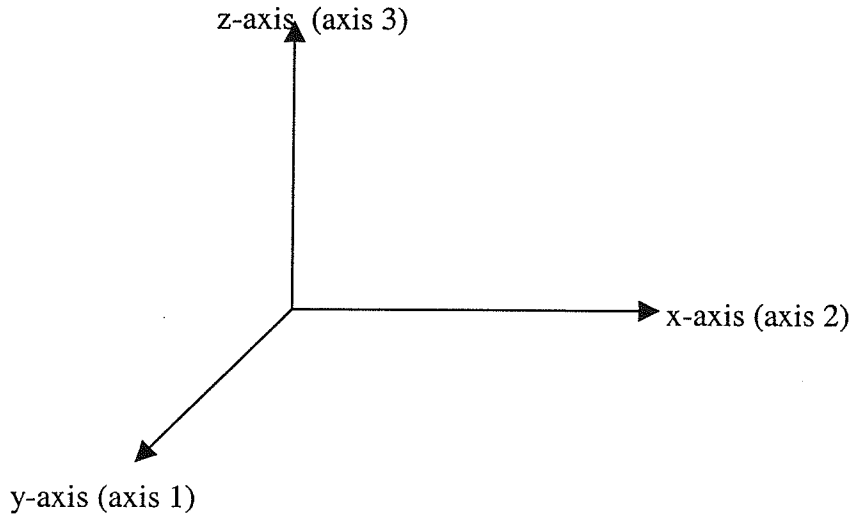

Figure 4.3 Indicates the directions the of the movement of the hydrophone

The program in Matlab calculates the acoustic pressure from the voltage using the calibration factor of the hydrophone. The calibration factor of 0.0425 V/MPa was used for this experiment. The collected data are read using the processing program which then calculates the *PII,* determines the maximum compressional pressure (P_c) and minimum rarefactional pressure at the focus, and finally plots a smooth curve of each. The RF hydrophone waveforms are processed to yield axial profiles for the above quantities. The purpose of smoothing is to eliminate the noise so that the peak of the curve would correspond to the maximum value instead of the noise spike[5]. The waveform representing the maximum value of the *PII* curve is also analyzed using Matlab (The Mathworks, Natick, MA). At least five independent calibrations for each voltage setting are performed.

The PII is the basic field quantity used to estimate the beam axis and is determined from equation 21 where the limits of integration are the duration of the pulse. The PII is determined for

each pulse by the same computer that controls the micropositioning system and acquires the digitized hydrophone voltage.

CHAPTER 5

EXPERIMENTAL RESULTS

This chapter presents the experimental results obtained using the procedures described in Chapter 4. The characterization results, by the wire technique, are listed in table5.1 for Fountain Transducer1 (FT#1) and Fountain Transducer 2 (FT#2).

Pulse-echo quantity	Transducer 1	Transducer 2
Center frequency (MHz)	3.0	3.32
Fractional bandwidth (%)	3.78	3.37
Focal length (mm)	126	137
-6-dB focal beamwidth (mm)	5.43	5.70
-6dB depth of focus (mm)	29.9	24.4

TABLE 5.1 Water-based pulse-echo ultrasonic field distribution results for 5.5-cm diameter transducer 1 and 6.0-cm diameter transducer 2.

The purpose of the fountain experiment is to determine the threshold voltage at which the the water-air interface fractures. From the fountain experiment, the distances are measured at the point when the water-air interface fractures. The distance is the interval between the transducer surface to the water-air interface. Corresponding voltage at which the surface is fractured at continuous acoustic wave conditions is also recorded and plotted in figure 5.1-5.2. A given voltage breaks the surface initially at a certain distance. As water is taken away from the tank, the distance decreases and the surface breakage amplifies creating initially droplets followed by mist and then a fountain. A picture depicting the dimple in the surface before the surface breaks is illustrated in figure 5.3. An illustration of the breakage in the surface is in figure 5.4 and an illustration of the amplification of the fountain is depicted in figure 5.5. As more water is taken out of the tank, the fountain decreases in amplitude and eventually the surface barely breaks again. The distance at which the surface barely breaks the water-air interface is then recorded. Therefore, for a given voltage, there are two distances that can break the water-air interface. As the voltage decreases, the range between the maximum

distance away from the transducer surface and the minimum distance away from the transducer surface to the water-air interface diminishes. However, the only voltage value of interest is the threshold or minimum voltage that is required to break the water-air interface. The results of the required voltage to break the water-air interface for pulsed acoustic wave is illustrated in figure 5.6-5.7.

Calibration of the transducer at some of these voltages is employed to determine the exact acoustic pressure at which the water-air interface is broken. From the first order acoustic pressure values, second order values can be determined such as PII, , I(TA), and $P_{rad.}$ The results of at least five independent calibrations are shown in the appendix in figure A.1 all the way to figure A.16 at the first and third harmonic frequency of each transducer. The results show that at lower voltage settings, the calibrations are more consistent than at higher voltage. As the voltage is increased, the acoustic wave becomes non-linear. In the non-linear region, the Pc, Pr, and PII become unpredictable. Calibrations of voltage settings below the threshold voltage at which the water-air surface breaks are carried out to test the consistency of the calibration in the linear region. The results of the calibrations at the voltage settings near the threshold voltage at which the water-air interface breaks are listed in figure 5.8-5.11. The average maximum PII value for the 5 independent calibrations and their standard deviation are shown in figure 5.12-5.15. These are the maximum PII values near the threshold voltage for transducer 1 (FT#1) and transducer 2 (FT#2) at the first and third harmonic frequency of each transducer.

The distance corresponding to the threshold voltage measured in the fountain experiment is compared to the distance at which the maximum PII occurs in the calibration. The results in figure 5.16 show that the distance from the surface of the transducer to the water-air interface corresponding to the threshold voltage is equivalent to the distance at which the maximum PII occurs from the calibrations.

For FT#1 at 3MHz, the minimum voltage required to break the water-air surface is 24.4 mV and the corresponding average distance is 13.6cm. From the calibration, the average distance at which the PII maximum occurs is 13.98cm with a standard deviation of 0.34cm.

For FT#2 at 3.32 MHz, the minimum voltage required to break the surface is 18.3mV and the corresponding average distance is 14.9cm. From the calibration, the distance at the PII maximum occurs at an average distance of 15.2 cm with a standard deviation of 0.3 cm.

The minimum voltage to break the water-air surface for FT#1 at 9MHz is 154mV and the corresponding distance is 14.75cm. From the calibrations, the average distance at which the PII maximum occurs is 14.95cm with a standard deviation of 0.66cm.

For FT#2 at 10MHz, the minimum voltage to break the surface is 209mV and the corresponding distance is 14.85cm. From the calibration the distance at the PII maximum is 14.75cm with a standard deviation of 0.13cm.

Table 5.2 summarizes the threshold voltage for each transducer at the first and third harmonic frequency penetrating the water-air interface.

Transducer	Frequency (MHz)	Threshold Voltage (mV)
FT#1	3.0	24.4
FT#1	9.0	154
FT#2	3.32	18.3
FT#2	10.0	209

TABLE 5.2 Threshold voltage at which the water-air interface fractures.

Table 5.3 indicates the minimum I(TA) required to break the water-air interface. I(TA) is obtained from dividing PII by the PD. The PII is the one corresponding to the threshold voltage. For FT#1 the I(TA) is statistically the same for the first and third harmonic frequency. For FT#2, the I(TA) for the third harmonic frequency is slightly greater than the I(TA) for the first harmonic frequency. However, the results do not indicate a significant difference.

Transducer	Frequency (MHz)	Threshold I(TA) (W/m^2)	Standard Deviation
FT#1	3.0	2.05E-4	3.05E-4
FT#1	9.0	7.27E-4	1.67E-4
FT#2	3.32	3.58E-4	2.85E-5
FT#2	10.0	1.68E-3	3.23E-4

TABLE 5.3 Threshold I(TA) required to break the water-air interface.

Table 5.4 indicates the minimum radiation pressure required to break the surface for both transducers at the first and third harmonic of each transducer. The radiation pressure is determined from dividing the I(TA) values obtained from table 5.3 by speed of sound in water (equation 3). No consistent trend is accomplished when both transducers are compared due to the large standard deviations at the focus. It appears that even at the focus, the acoustic wave is still non-linear in nature and the maximum PII has large fluctuations in some cases. Therefore, the fracture in the water-air interface does not seem to depend on frequency.

Transducer	Frequency (MHz)	Threshold P_{rad} (N/m^2)	Standard Deviation
FT#1	3.0	1.38E-7	2.05E-7
FT#1	9.0	4.90E-7	1.12E-7
FT#2	3.32	2.41E-7	1.92E-8
FT#2	10.0	1.13E-6	2.18E-7

TABLE 5.4 Threshold radiation pressure required to break the water-air interface.

The investigation of pulsed acoustic wave application to the water-air interface is indicated in tables 5.5 and 5.6. For FT#1, as the PRP increases, the I(TA) and radiation pressure either increase or decrease. The large standard deviation for FT#1 makes the relationship between I(TA) and PRP inconclusive, and similarly for radiation pressure.

Transducer	Frequency (MHz)	PRP (μs)	I(TA) (W/m^2)	P_{rad} (N/m^2)
FT#1	3.0	30	1.63E-3	1.01E-6
FT#1	3.0	60	1.46E-3	9.82E-7
FT#1	3.0	90	1.52E-3	1.02E-6
FT#2	3.32	30	3.33E-3	2.24E-6
FT#2	3.32	60	3.50E-3	2.36E-6
FT#2	3.32	90	4.10E-3	2.77E-6

TABLE 5.5 Threshold I(TA) and P_{rad} required to break the water-air interface at pulsed condition.

For FT#2, as the PRP increases, the I(TA) is statistically the same, and similarly for the radiation pressure. The PII corresponding for the threshold voltages in the pulsed experiments are interpolated from the plots in figure A.7-A.8.

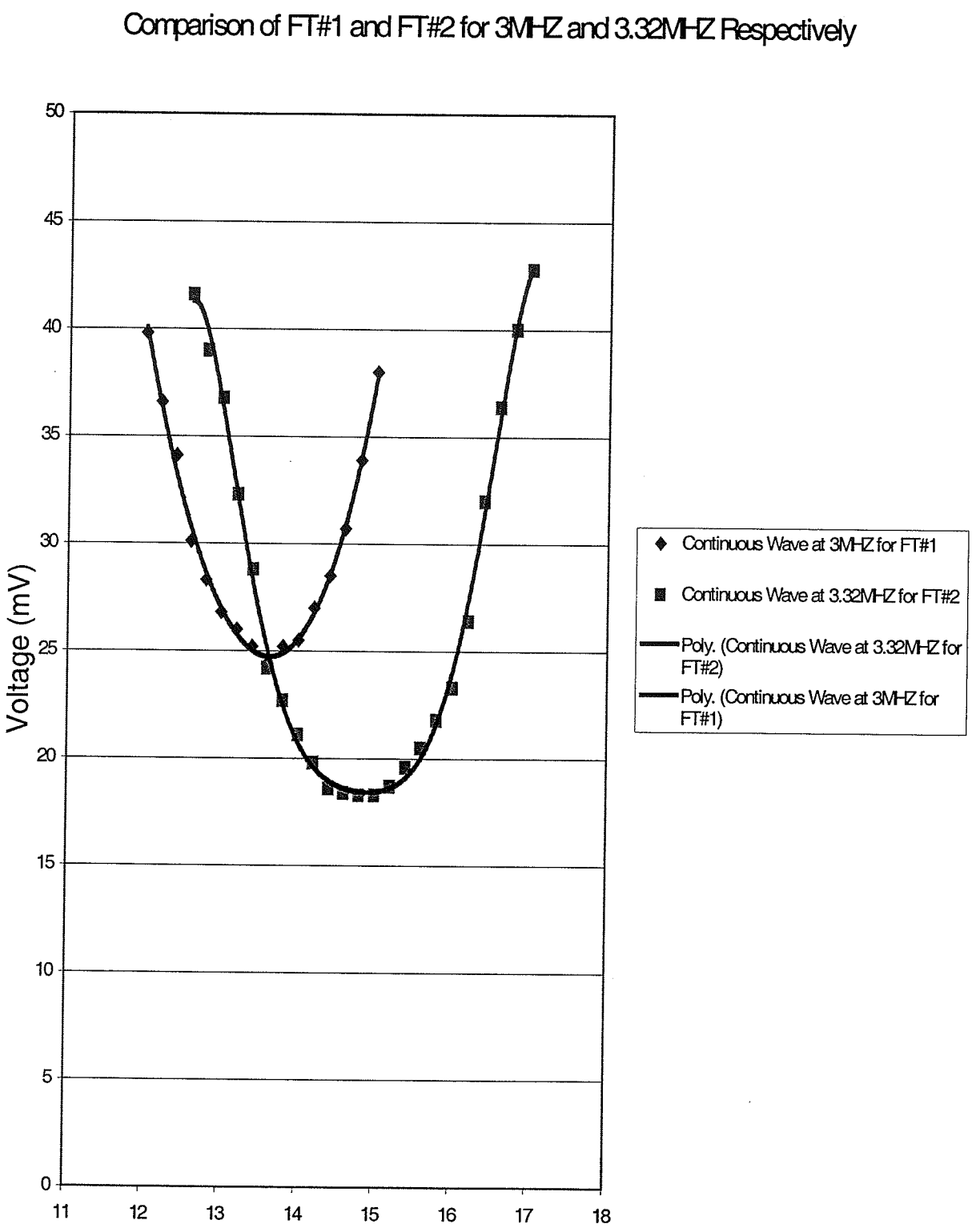

Figure 5.1 Curve that shows the voltage that breaks the water-air interface. The minimum voltage is threshold voltage that breaks the water surface. These results are for the first harmonic frequency of each transducer.

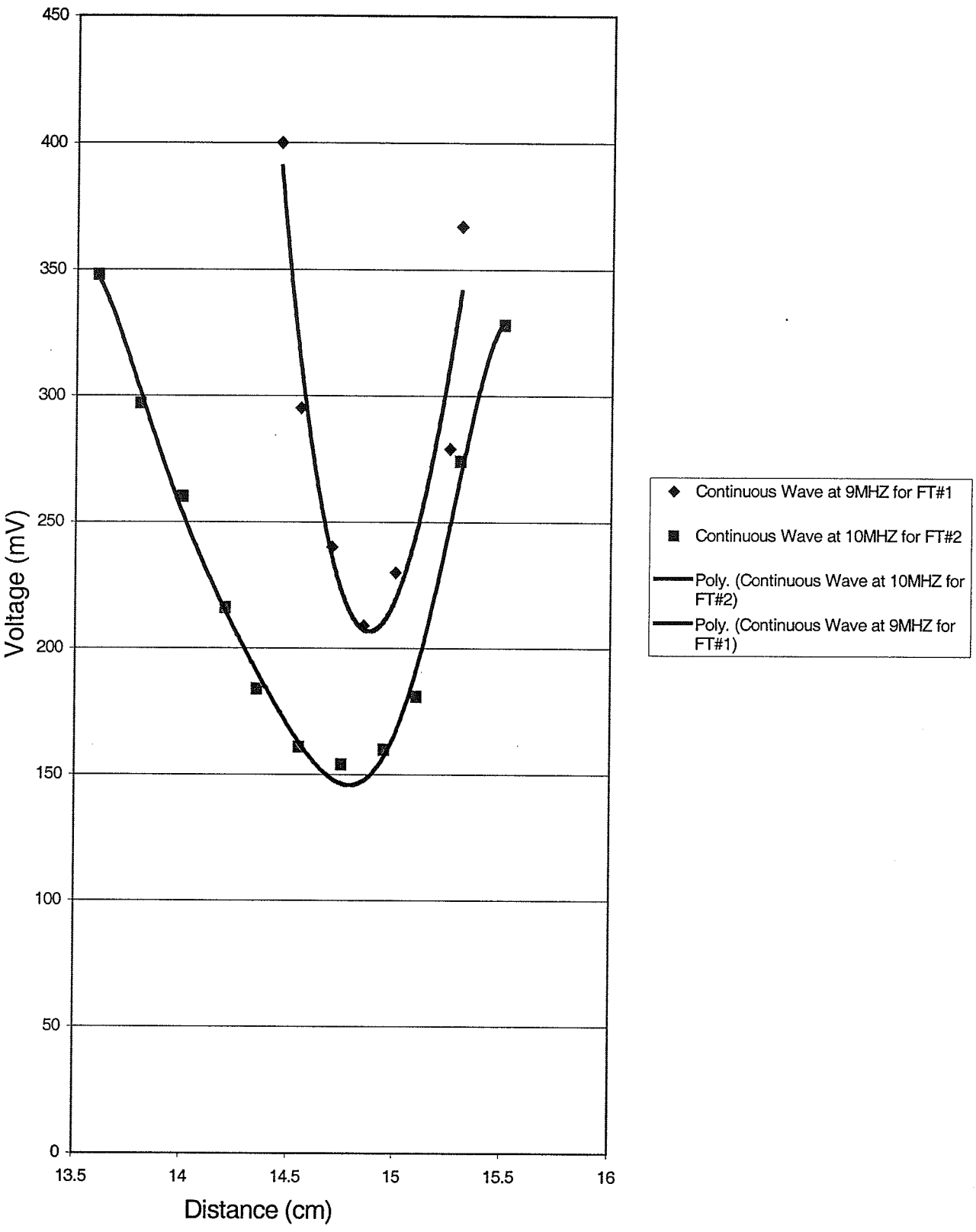

Figure 5.2 Curve that shows the voltage that breaks the water-air interface. The minimum voltage is threshold voltage that breaks the water surface. These results are for the third harmonic frequency of each transducer.

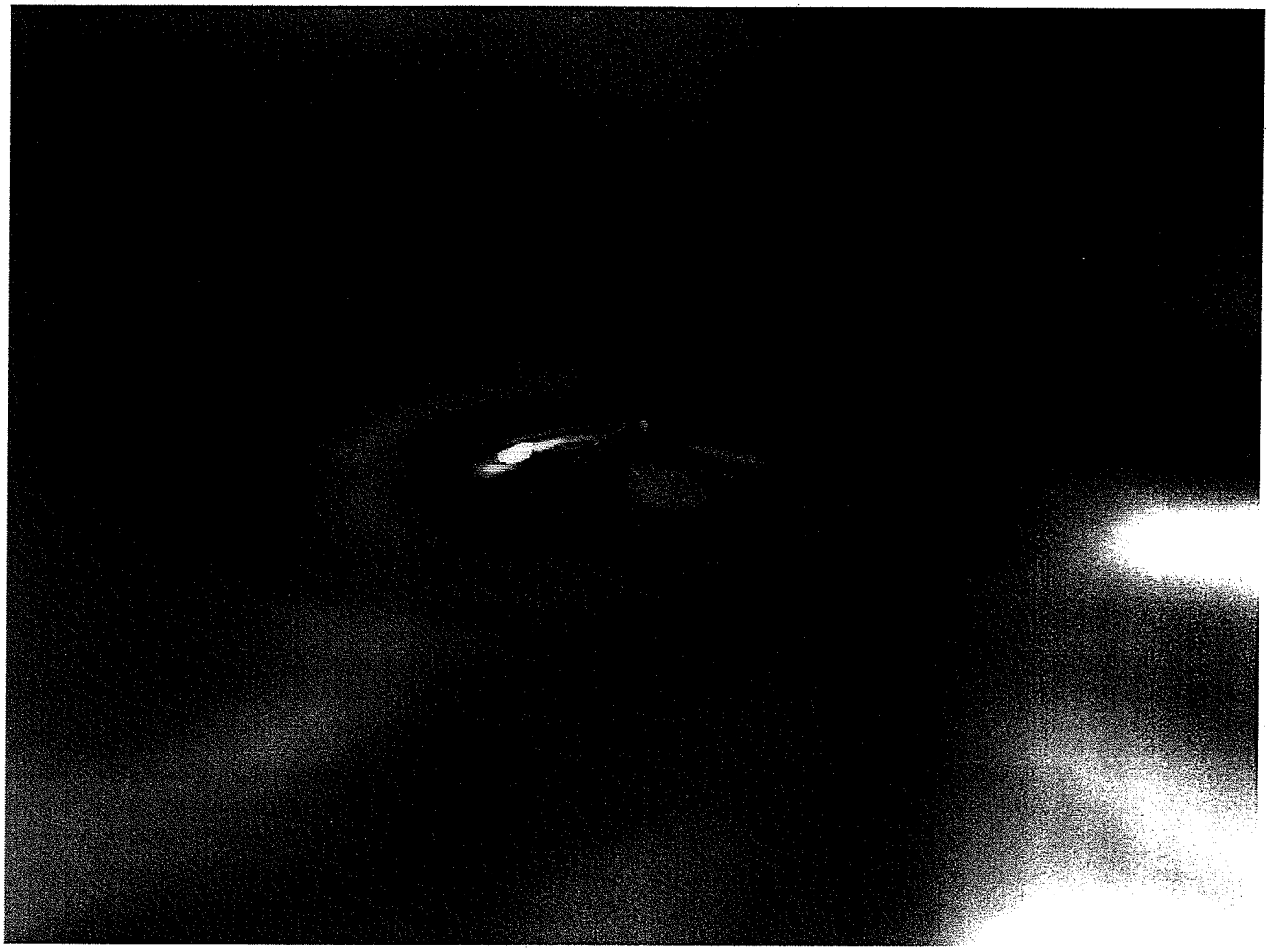

Figure 5.3 Indicates a picture of the dimple before a fracture occurs.

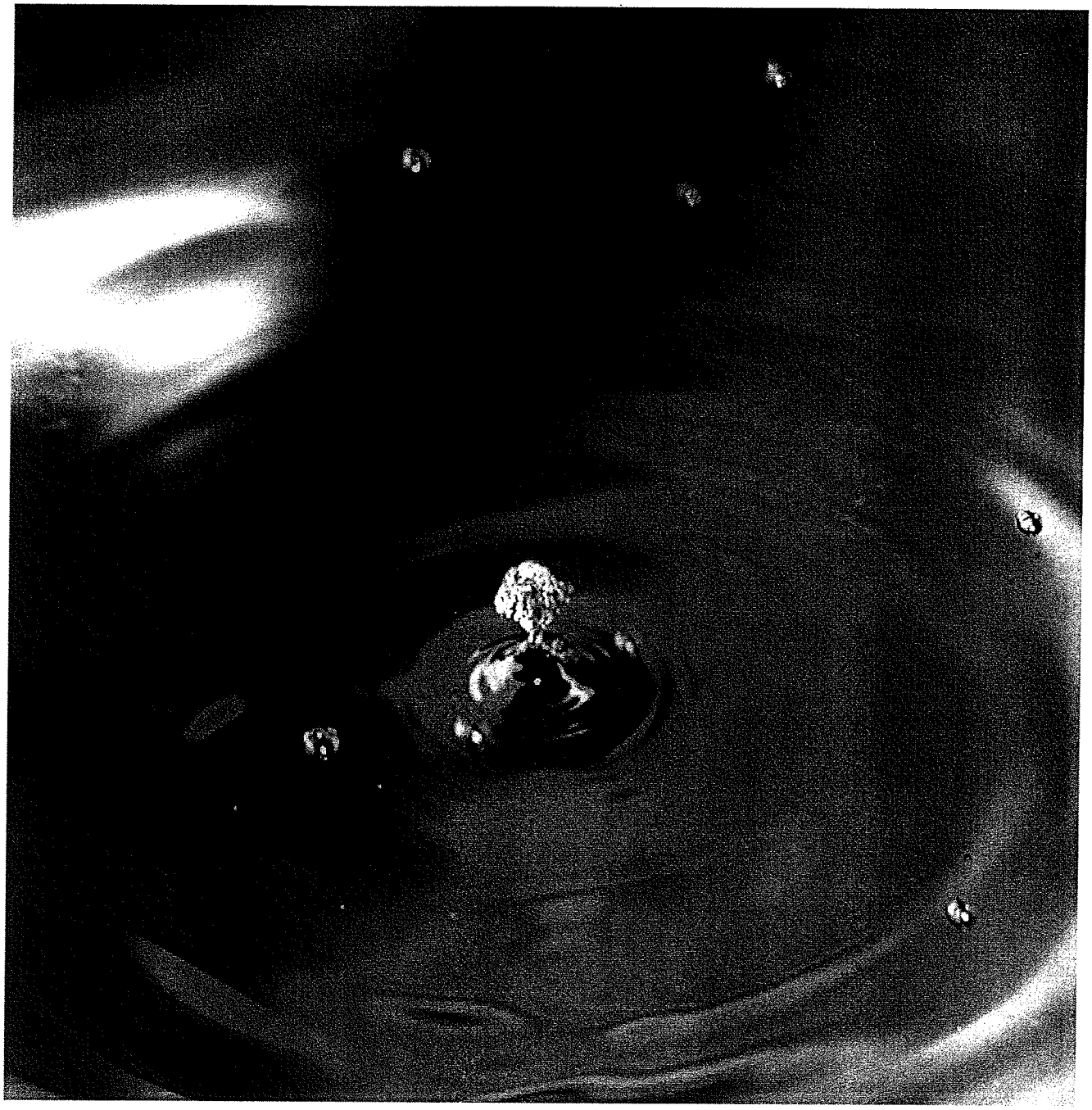

Figure 5.4 Indicates a picture of the fracture in the water-air interface.

Figure 5.5 Indicates a picture of the amplified fountain effect and the mist.

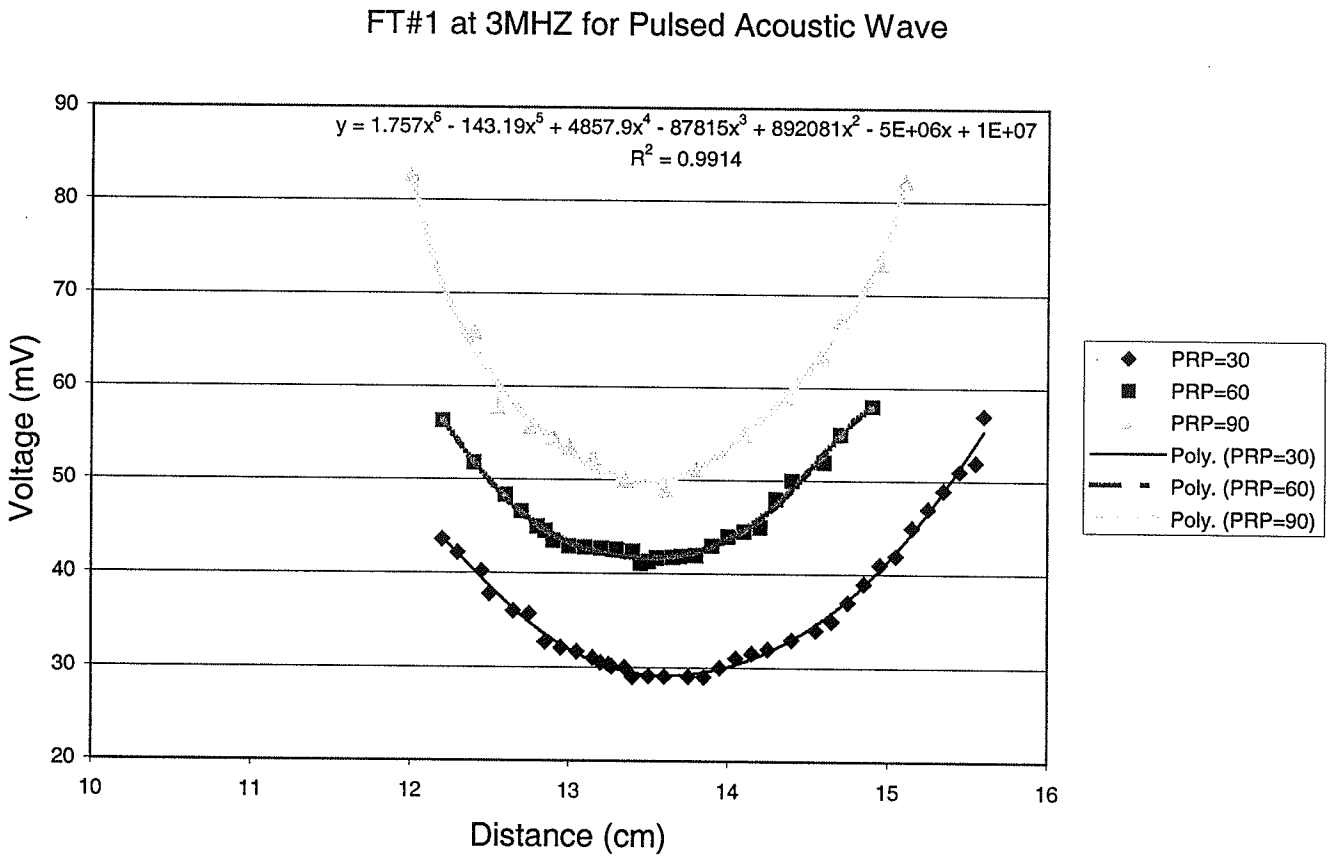

Figure 5.6 Determines the minimum voltage that is required to break the water-air interface at pulsed acoustic wave for FT#1.

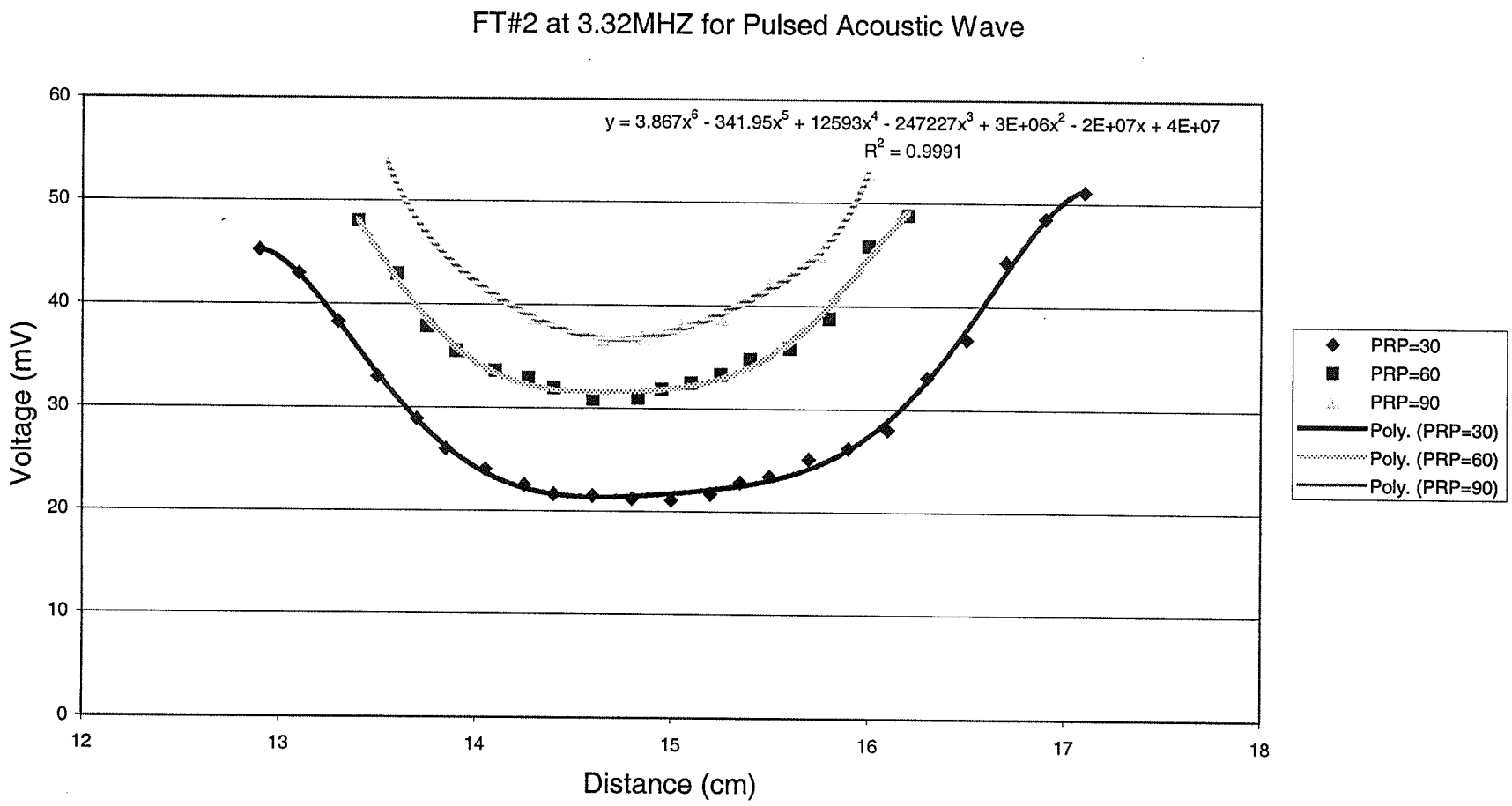

Figure 5.7 Determines the minimum voltage that is required to break the water-air interface at pulsed acoustic wave for FT#2.

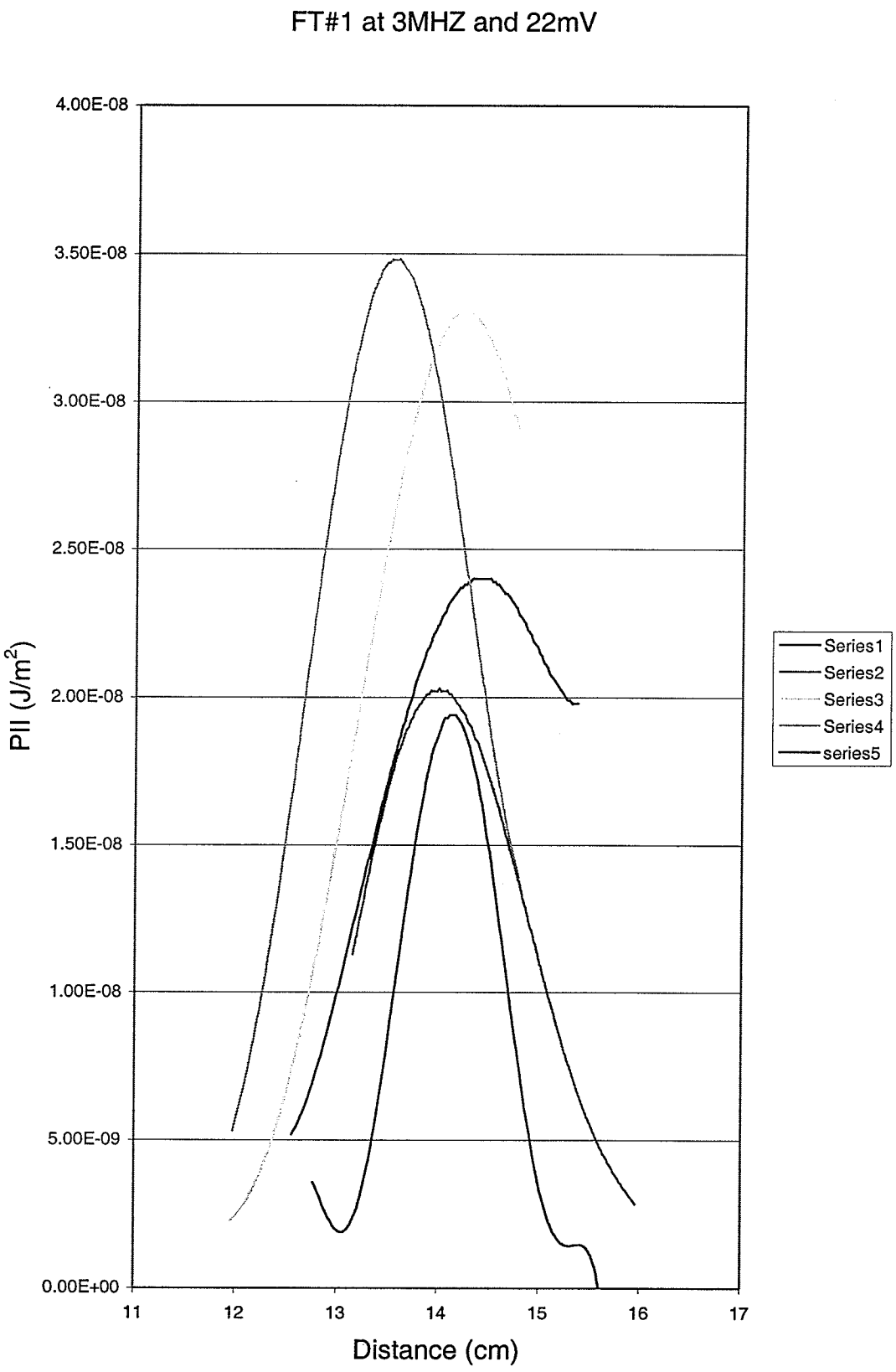

Figure 5.8 PII curves for 5 independent calibrations for a voltage of 22mV. This is the closest calibrated voltage to the threshold of 24.4mV at which the surface is fractured.

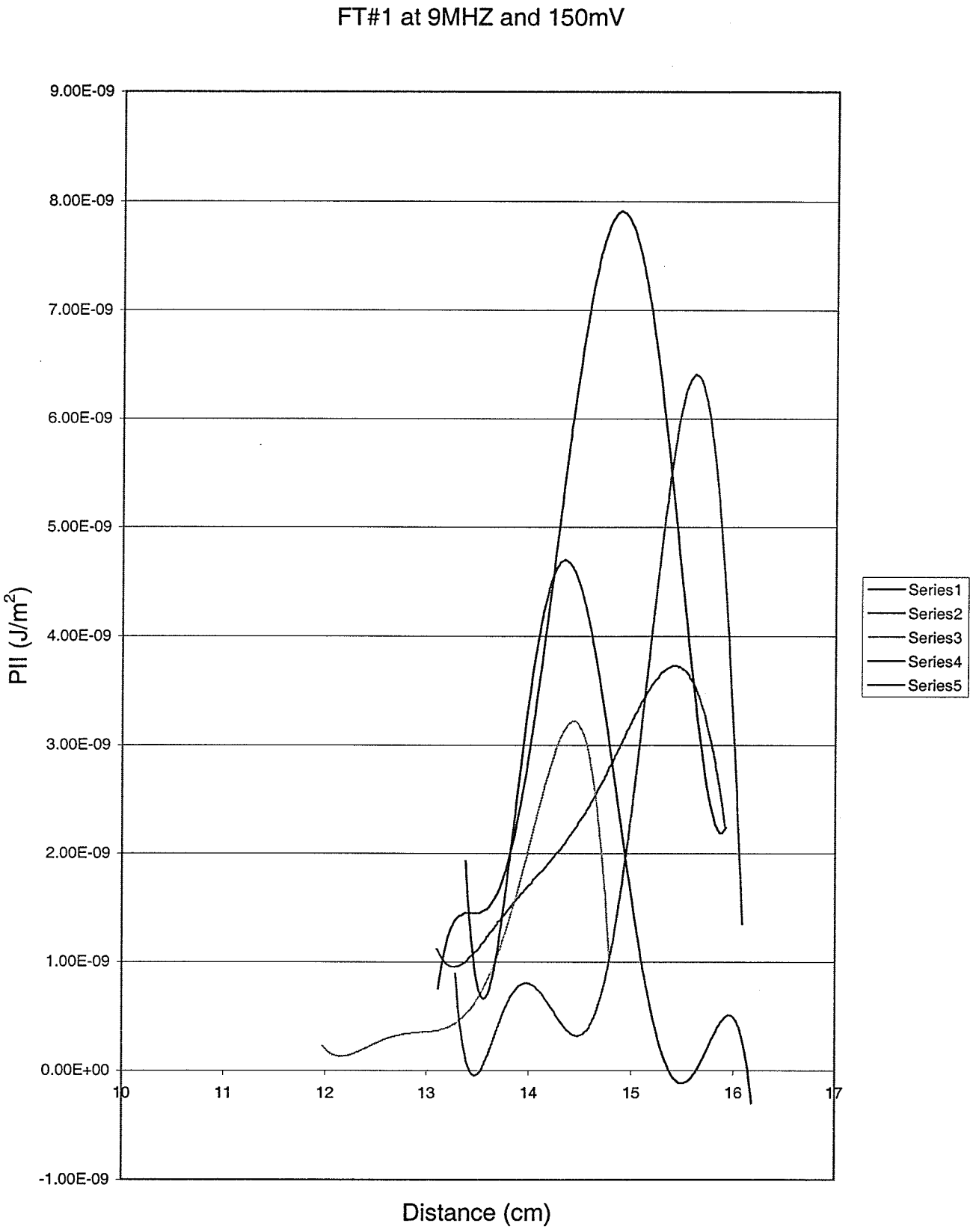

Figure 5.9 PII curves for five independent calibrations for a voltage of 150mV. This the closest calibrated voltage to the threshold voltage of 154mV at which the water-air interface is fractured.

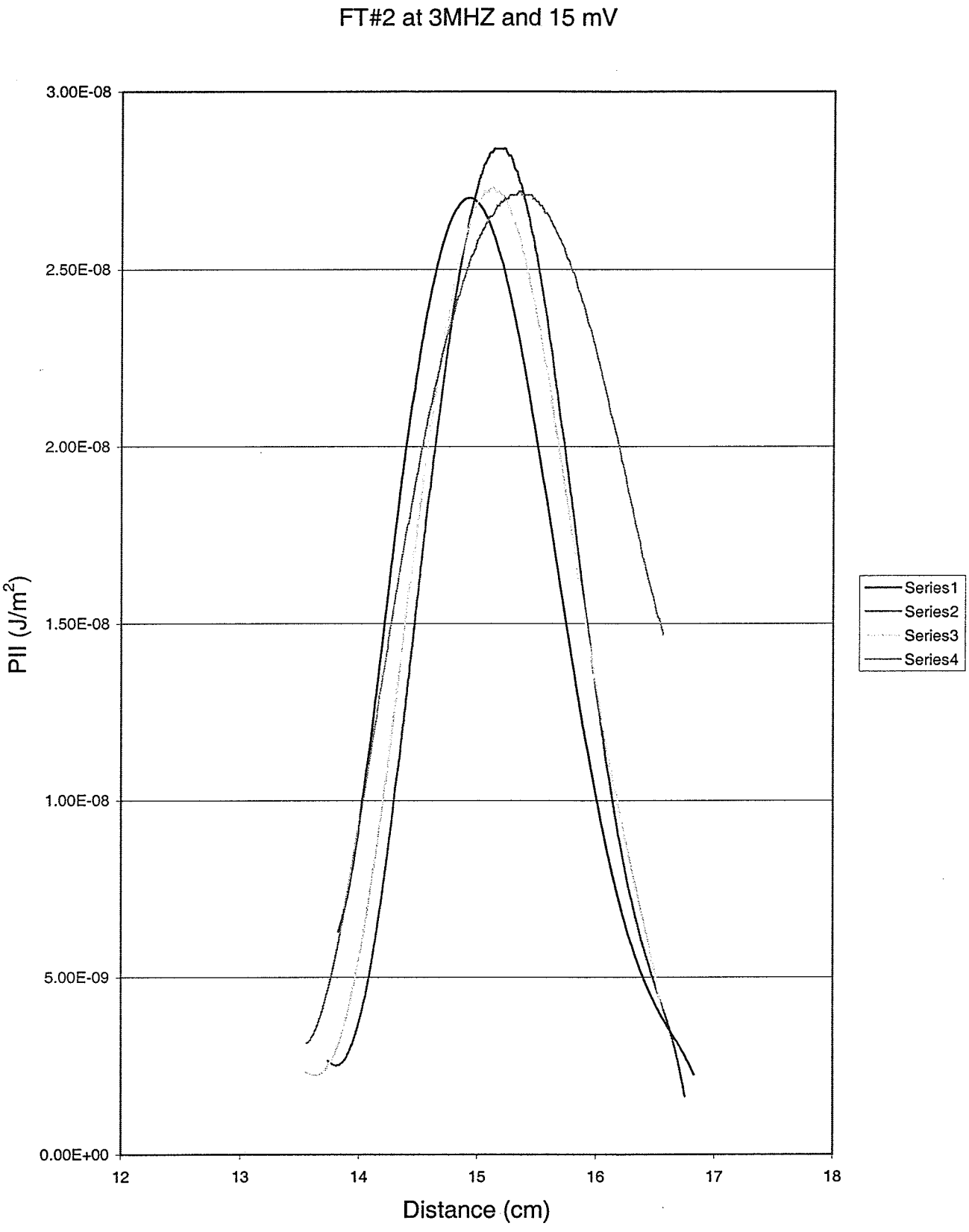

Figure 5.10 PII curves for four independent calibrations at a voltage of 15mV. This is the calibrated voltage to the threshold voltage of 18.3mV at which the water-air interface is fractured.

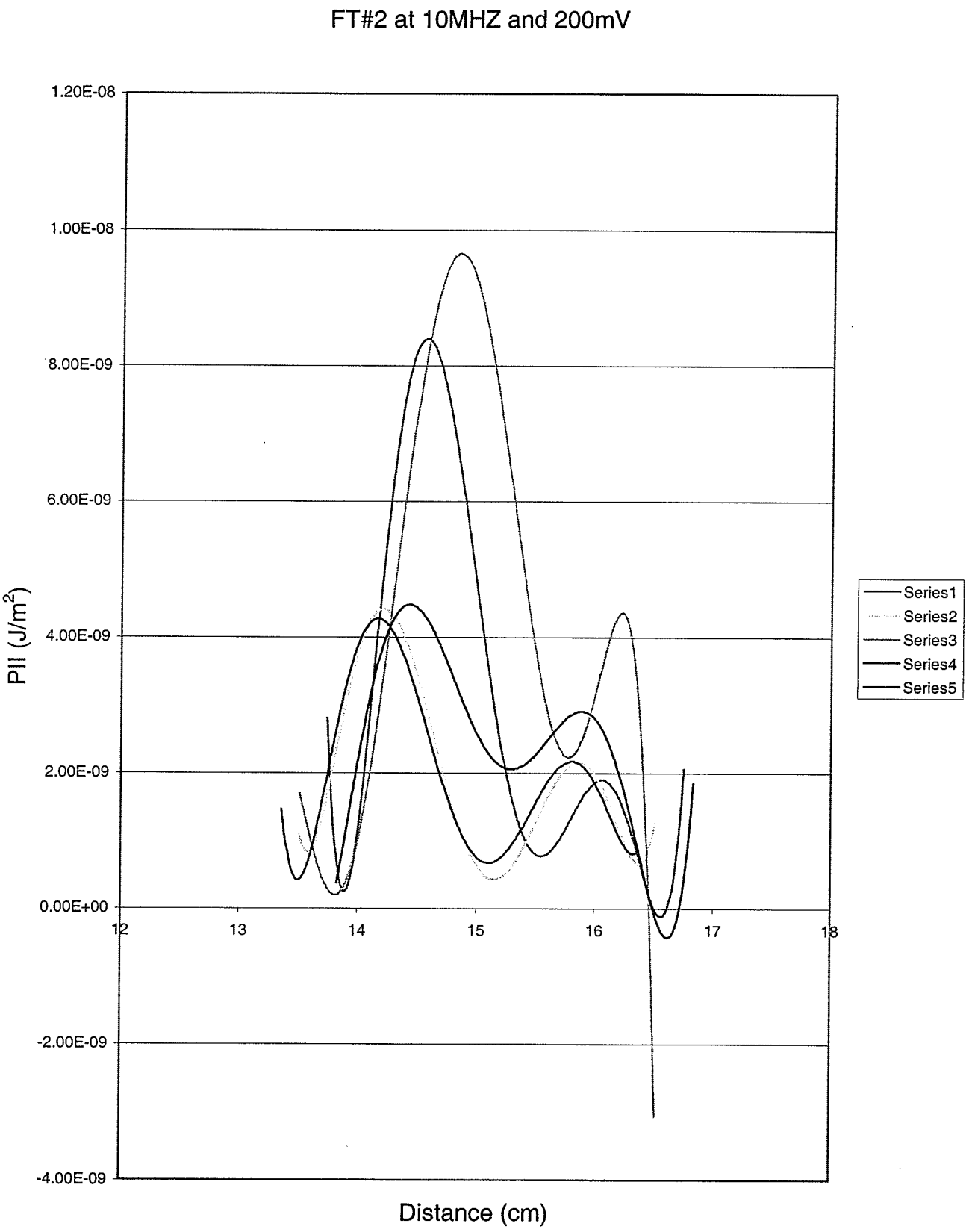

Figure 5.11 PII curves for five independent calibrations at voltage of 200mV. This the closest calibrated voltage to the threshold voltage of 209mV at which the water-air interface is fractured.

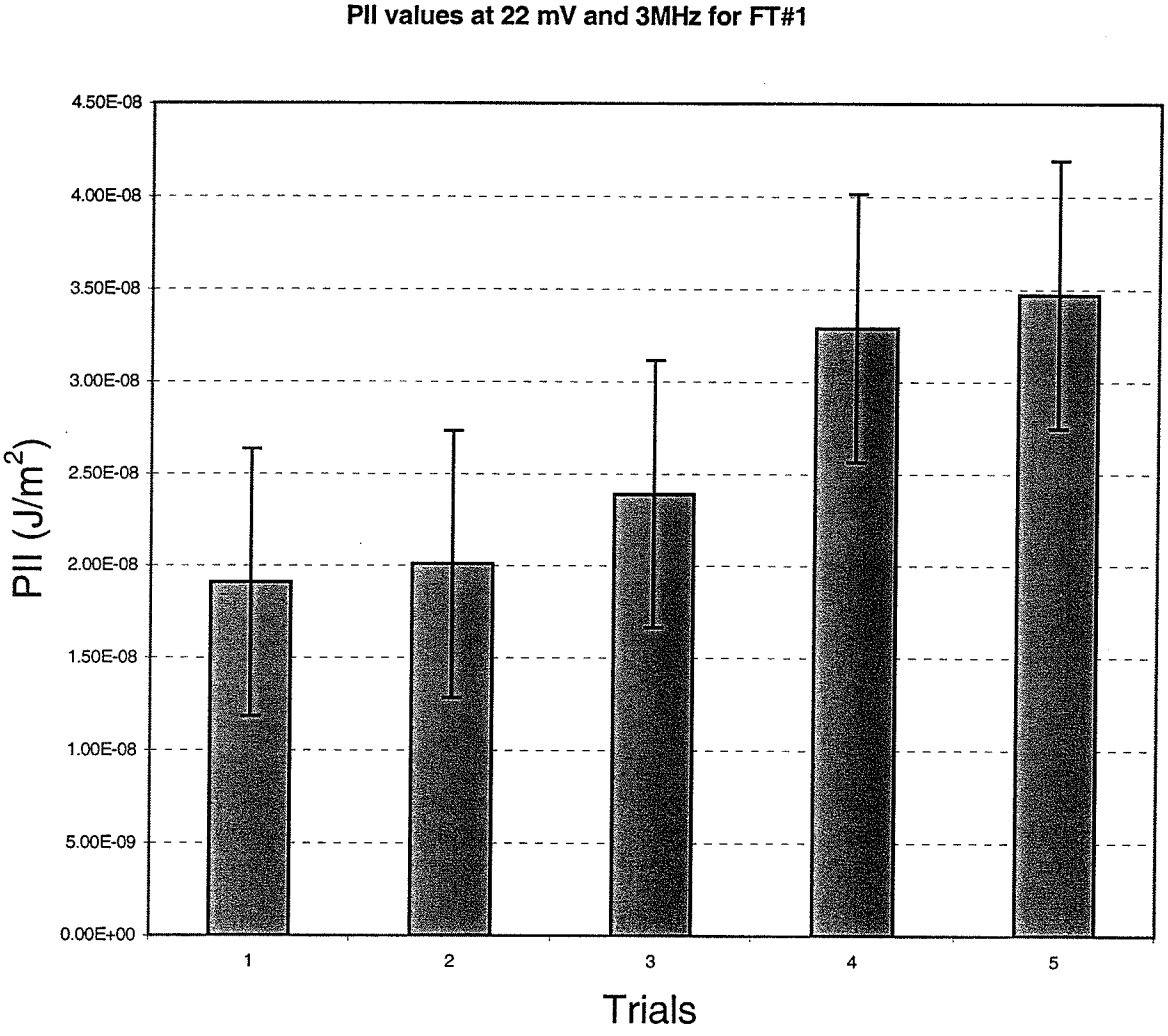

Figure 5.12 Maximum PII values for five independent calibrations at 22mV. The standard deviation is 7.246E-9.

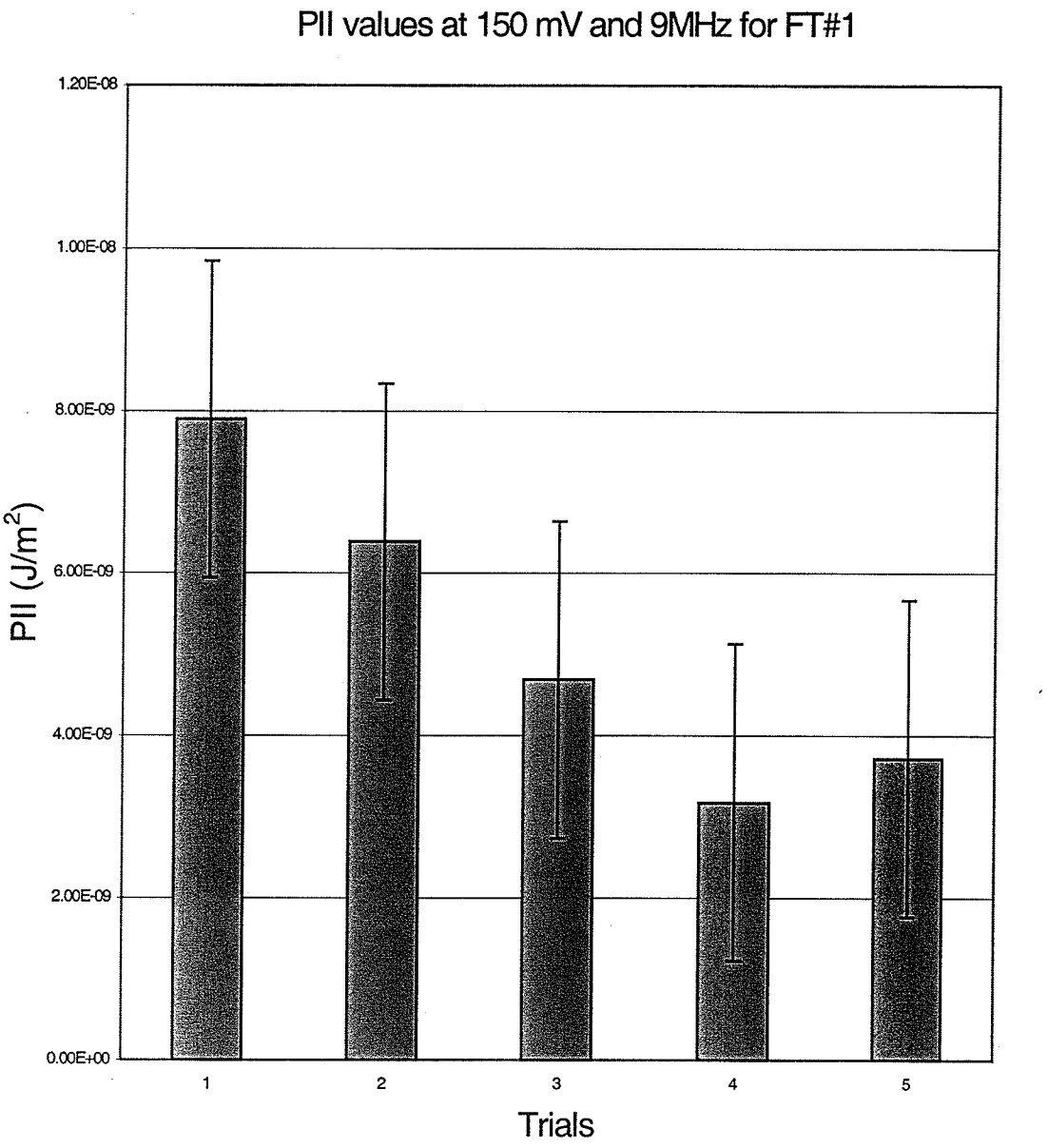

Figure 5.13 Maximum PII values for 5 independent calibrations at 150mV. The standard deviation is 1.95E-9.

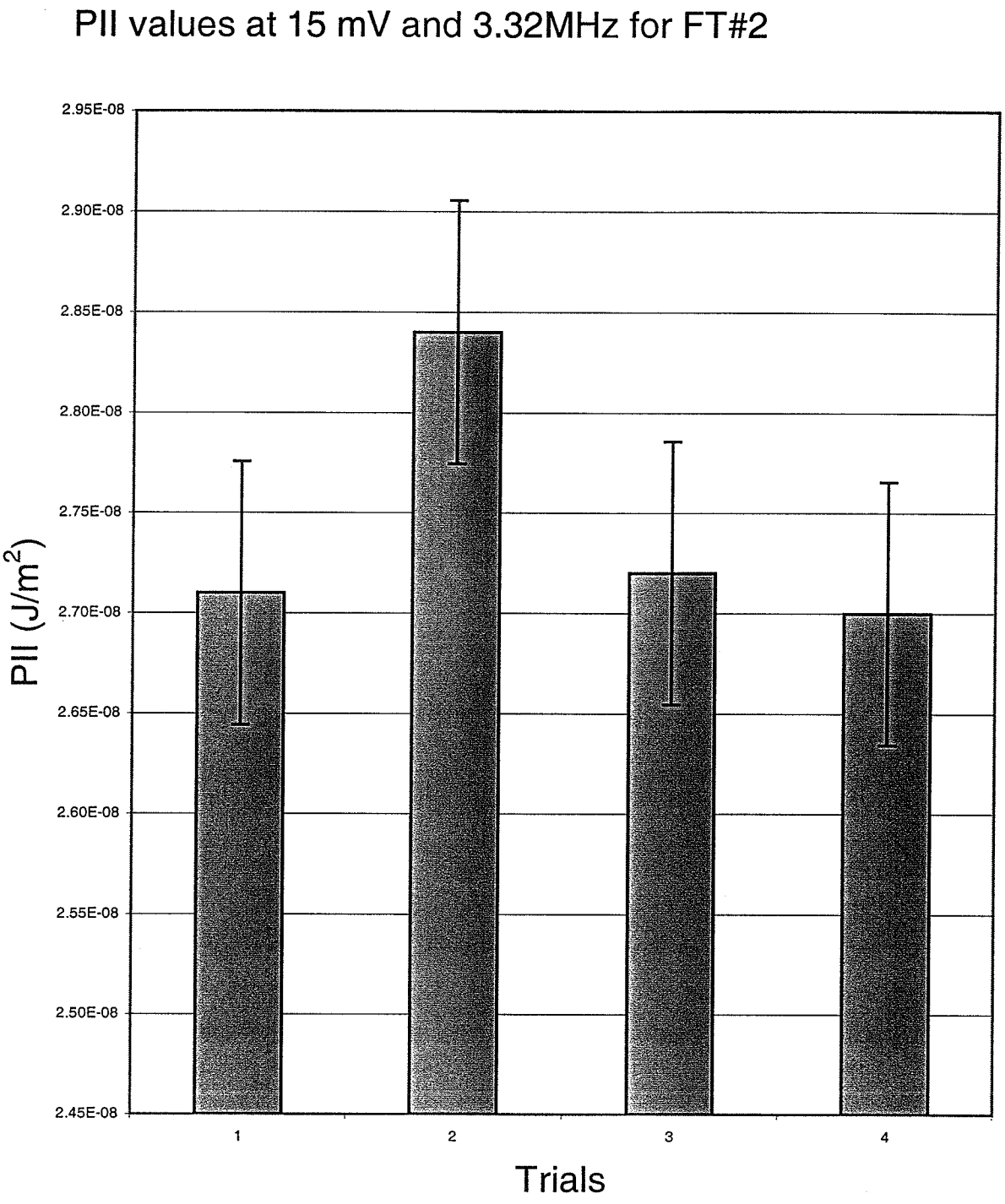

Figure 5.14 Maximum PII values for 4 independent calibrations at 15mV. The standard deviation is 6.55E-10.

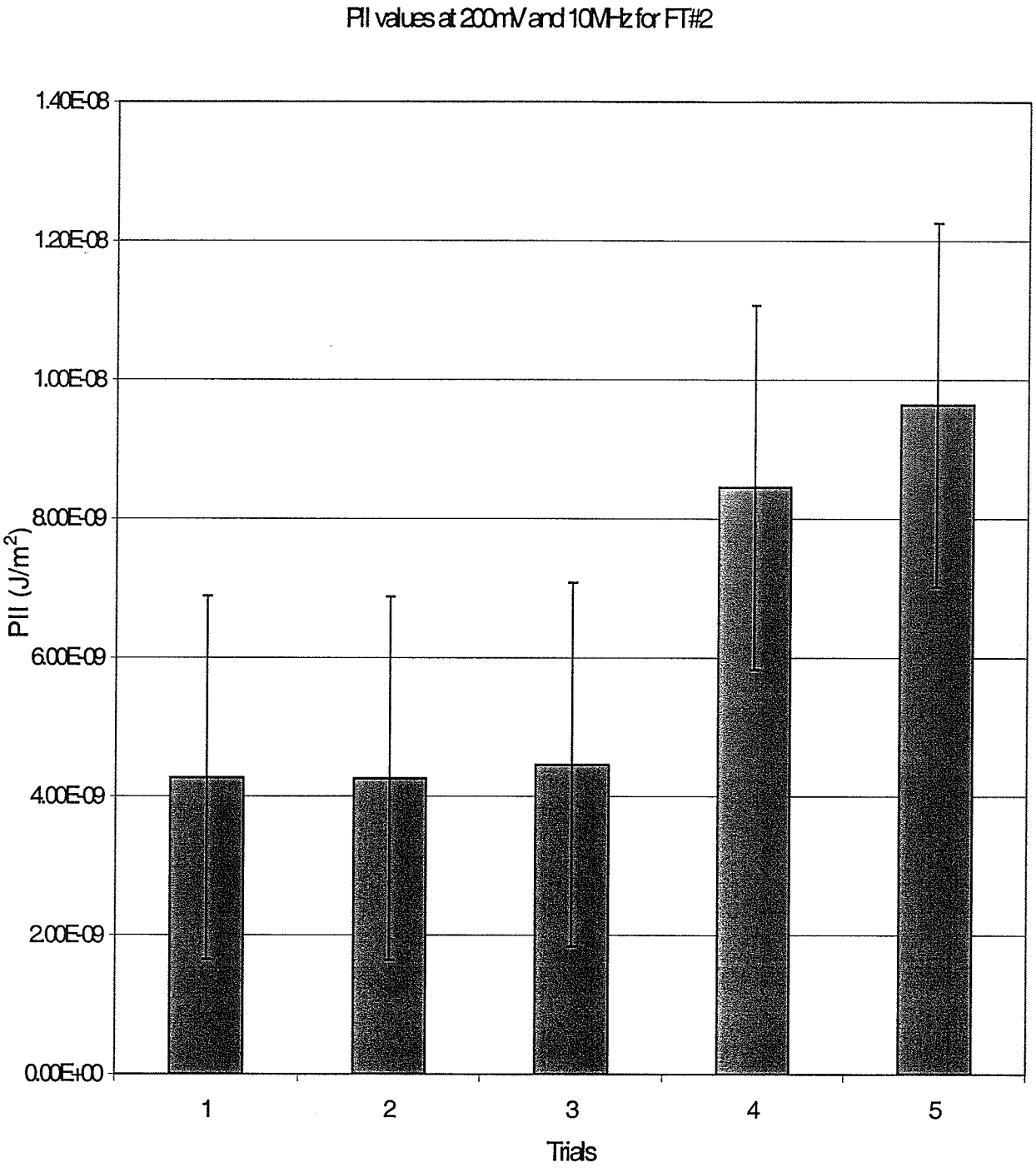

Figure 5.15 Maximum PII values for 5 independent calibrations at 200mV. The standard deviation is 2.62E-9.

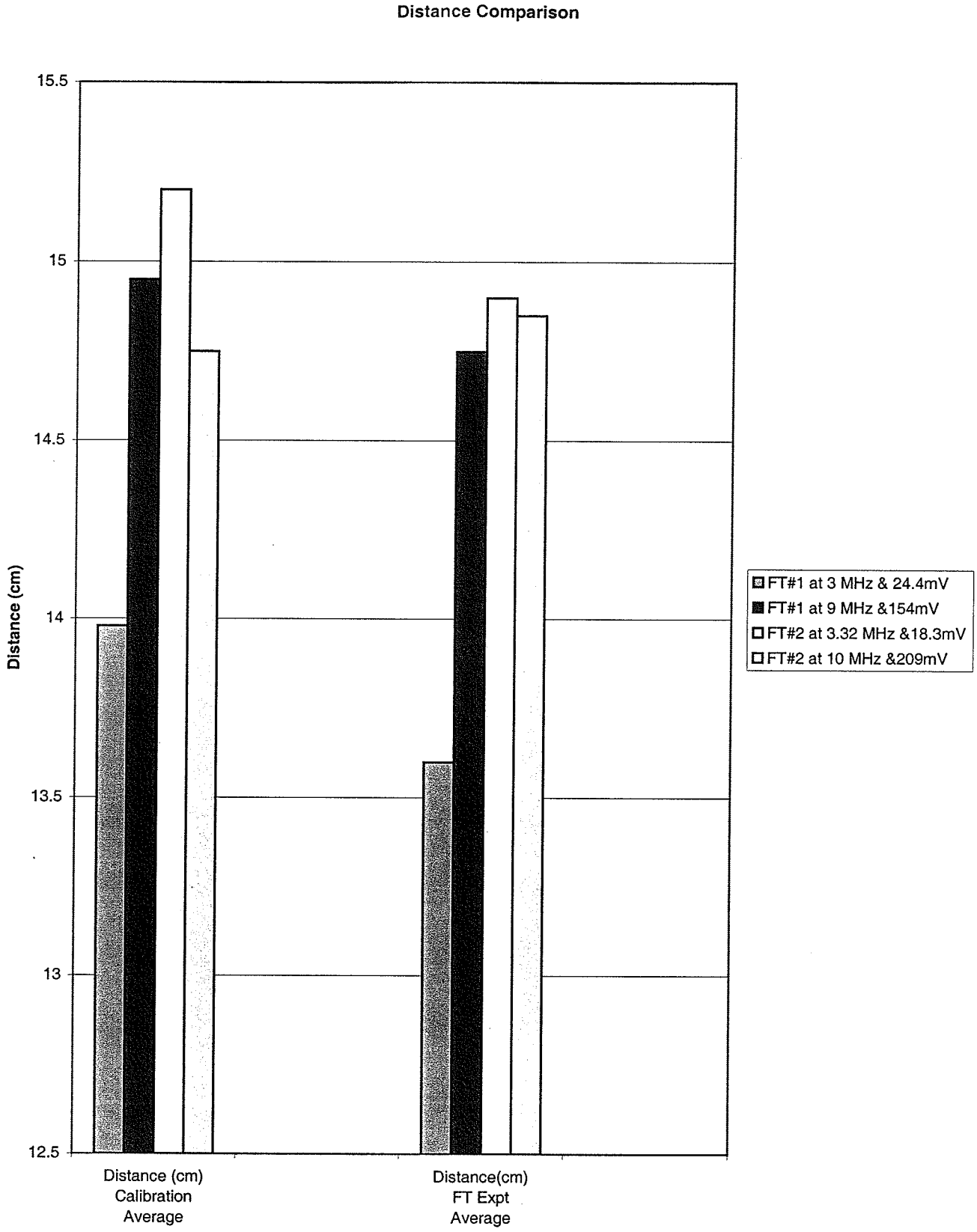

Figure 5.16 The average distance at which the maximum PII occurs obtained from the 5 independent calibrations are compared to the distance at which the water surface breaks in the fountain experiment.

CHAPTER 6

DISCUSSIONS AND CONCLUSIONS

The purpose of the fountain experiment is to determine whether radiation pressure is possible mechanism for the fracture in the water-air interface. First the minimum voltage that is necessary for the breakage of the water-air interface is obtained from the experiment. From the calibrations, the voltage is converted into a PII value and in turn I(TA) and radiation pressure.

The minimum radiation pressure that is required to break the water-air interface occurs at the focus of the beam because of two reasons. Firstly, the beam-width of the beam at the focus is smallest compared to the beam-width of the rest of the beam; thus, the minimum voltage and in turn radiation pressure should be able to break the surface at that point. As the beam diverges, more voltage is required to break the surface. Secondly, as indicated in figure 5.16, the maximum PII and in turn the radiation pressure obtained from the calibrations is occurring at the same position at which water-air interface is broken. Because the maximum radiation pressure occurs at the same location the water-air interface breaks, it is assumed that radiation pressure is indeed a mechanical effect that is responsible for the fracture in the water-air interface and in turn the ultrasound-induced lung hemorrhage.

The pulsed experiments reported in figure 5.6-5.7 and summarized in table 5.5 indicate that the I(TA) remains statistically constant as the PRF varies. Because a threshold constant energy value is required to cause a fracture in the surface, the fact that the I(TA) and in turn radiation pressure remains constant as the PRF varies proves that radiation pressure or I(TA) is responsible for the breakage in the water-air interface. Since a certain amount of radiation pressure is required to break the water-air interface, theoretically the radiation pressure must remain constant as the PRF is varied. This means that the PII must increase to compensate for a decrease in PRF. In conclusion, pulsed

experiments show that the I(TA) and in turn, the radiation pressure required to break the water-air interface is statistically constant.

The fracture does not seem to depend on frequency. I(TA) and in turn, radiation pressure are statistically the same for both the first and the third harmonic frequency. Further work is needed to test whether the breakage in the water-air interface is beam-width dependent.

The water-air interface fracture simulates the fracture in the large gas bodies within tissues (such as air in the lung alveoli) or in tissue lacking cavitational nuclei. Therefore, the results can be extrapolated to ultrasound-induced lung hemorrhage.

SYMBOLS

ξ: *Particle displacement for a continuous wave*

ξ_0: *Particle displacement amplitude*

ω: *Angular frequency*

k: *Propagation constant*

t: *time*

U: *Particle velocity*

U_0: *Velocity amplitude*

A: *Particle acceleration*

A_0: *Acceleration amplitude*

P: *Acoustic pressure*

P_0: *Pressure amplitude*

W: *Acoustic power averaged over one or more cycles of a continuous wave*

C_0: *Speed of sound*

ρ_0: *Density of medium*

ΔE: *Total energy*

E_I: *Instantaneous energy*

E: *Energy density at any point in the fluid*

V_0: *Particle volume*

I: *Time-average intensity of a continuous wave*

I_I: *Instantaneous intensity*

PRF: Pulse repetition frequency

PRP: Pulse repetition period

PD: Pulse duration

PII: Pulse intensity integral

I(TP): Temporal peak intensity

I(PA): Pulse average intensity

I(TA): Temporal average intensity; intensity averaged over longer interval of PRP

DF: Duty factor

p_I: *Pulse-pressure-squared integral*

I(SA): Spatial average intensity

I(SP): Spatial peak intensity

I(SPTP): Spatial peak, temporal peak intensity

I(SPPA): Spatial peak, pulse average intensity

I(SPTA): Spatial peak, temporal average intensity

I(SATP): Spatial average, temporal peak intensity

I(SAPA): Spatial average, pulse average intensity

I(SATA): Spatial average, temporal average intensity

I_p: *Instantaneous peak intensity*

I_m: *Maximum intensity*

I_t: *I(SATA) at the transducer*

REFERENCES

[1] Biological Effects of Ultrasound: Mechanisms and Clinical Implications, *National Council on Radiation Protection and Measurements.* NCRP Report No. 74, 1983.

[2] Roy C. Preston, ED., *Output Measurements for Medical Ultrasound.* Springer-Verlag, 1991.

[3] L.E. Kinsler, A.R. Frey, A.B. Coppens, and J.V. Sanders, *Fundamentals of Acoustics.* John Wiley & Sons, 1982.

[4] W.R. Hendrick, D.L. Hykes, and D.E. Starchman, *Ultrasound Physics and Instrumentation.* Mosby, 1992.

[5] J.M. Semprott, "Experimental Evaluation of Acoustic Saturation," M.S thesis in Electrical Engineering at Universiy of Illinois at Urbana-Champaign, 2000.

[6] K. Biessner, 1984. Journal of Sound and Vibration **93**, 537-548. Acoustic Radiation Pressure in the Near Field.

[7] Boa-Teh Chu and Robert E. Apfel ,1982. Journal of Acoustical Society of America **72**,1673-1686. Acoustic Radiation Pressure Produced by a Beam of sound.

[8] Diane Dalecki, Carol H. Raeman, Sally Z. Child, and Edwin L. Cartensen, 1997. Ultrasound in Medicine and Biology **23**, 275-285. Effects of Pulsed Ultrasound on the Frog Heart: III. The Radiation Force Mechanism.

[9] Francis A. Duck and Hazel C. Starritt, 1986. Ultrasound in Medicine and Biology **12**(5), 403-409. The Locations of Peak Pressures and Peak Intensities in Finite Amplitude Beams From a Pulsed Focused Transducer.

[10] D.P Penney, E.A Schenk, K. Maltby, C. Hartman-Raeman, S.Z. Child and E.L. Cartensen, 1993. . Ultrasound in Medicine and Biology **19**(2) 127-135. Morphological Effects of Pulsed Ultrasound in the Lung.

[11] S.B. Barnette, G.R. Ter Harr, M.C. Ziskin, W.L. Nyborg, K. Maeda and J. Bang, 1994. . Ultrasound in Medicine and Biology **20**(3) 205-218. Current Status of Research on Biophysical Effects of Ultrasound.

[12] Kay Raum and William D. O'Brien, 1997. IEEE Transactions on Ultrasonics, Ferroelectrics, and Frequency Control **44**(4) 810-815. Pulse-Echo Field Distribution Measurement Technique for High Frequency Ultrasound Sources.

[13] William D. O'Brien, Jr., Leon Frizzell, Ronald M. Weigel, and James F. Zachary, 2000. Journal of Acoustical Society of America **108** (3) 1290-1297. Ultrasound-Induced Lung Hemorrhage is Not Caused by Inertial Cavitation.

[14] S.Z Child, C.L. Hartman, L.A. Schery, and E.L Cartensen, "Lung Damage from Exposure to Pulsed Ultrasound," Ultrasound Med. Biol. **16,** 817-825 (1990).

[15] C.L Hartman, S.Z. Child, R. Mayer, E. Schenk, and E.L. Cartensen, "Lung Damage from exposure to the fields of an electrohydraulic lithotripter," Ultrasound Med. Biol. **16,** 675-683 (1990).

[16] A.F. Tarantal and D.R. Canfield, "Ultrasound-Induced lung hemorrhage in the monkey," Ultrasound Med. Biol. **20,** 65-72 (1994).

[18] *Mechanical Bioeffects from Ultrasound*: AIUM *Consensus Statements* (American Institute of Ultrasound in Medicine, Laurel, MD, 2000). Also, J. Ultrasound Med. **19,** 67-168 (2000)

[19] C.K Holland, C.X. Deng, R.E. Apfel, J.L. Alderman, L.A. Fernandez, and K.J.W. Taylor, "Direct evidence of cavitation *in vivo* from diagnostic ultrasound," Ultrasound Med. **22,** 917-925 (1996)

[20] J.F. Zachary and W.D. O'Brien, Jr.,"Lung lesion induced by continuous and pulsed-wave (diagnostic) ultrasound in mice, rabbits, and pigs," Vet Pathol., **32,** 43-54 (1995)

[21] R. Baggs, D.P. Penney, C. Cox, S.Z. Child, C.H. Raeman, D. Dalecki, and E.L. Cartensen, "Thresholds for ultrasonically induced lung hemorrhage in neonatal swine," Ultrasound Med., **22,** 119-128 (1996)

[22] J.F. Zachary, J.M Sempsrott, L.A. Frizzell, D.G. Simpson, and W.D. O'Brien, Jr.,"Superthreshold behavior and threshold estimation of ultrasound-induced lung hemorrhage in adult mice and rats," IEEE Transactions on Ultrasonics, Ferroelectrics, and Frequency Control, **48**, 581-591 (2001)

APPENDIX

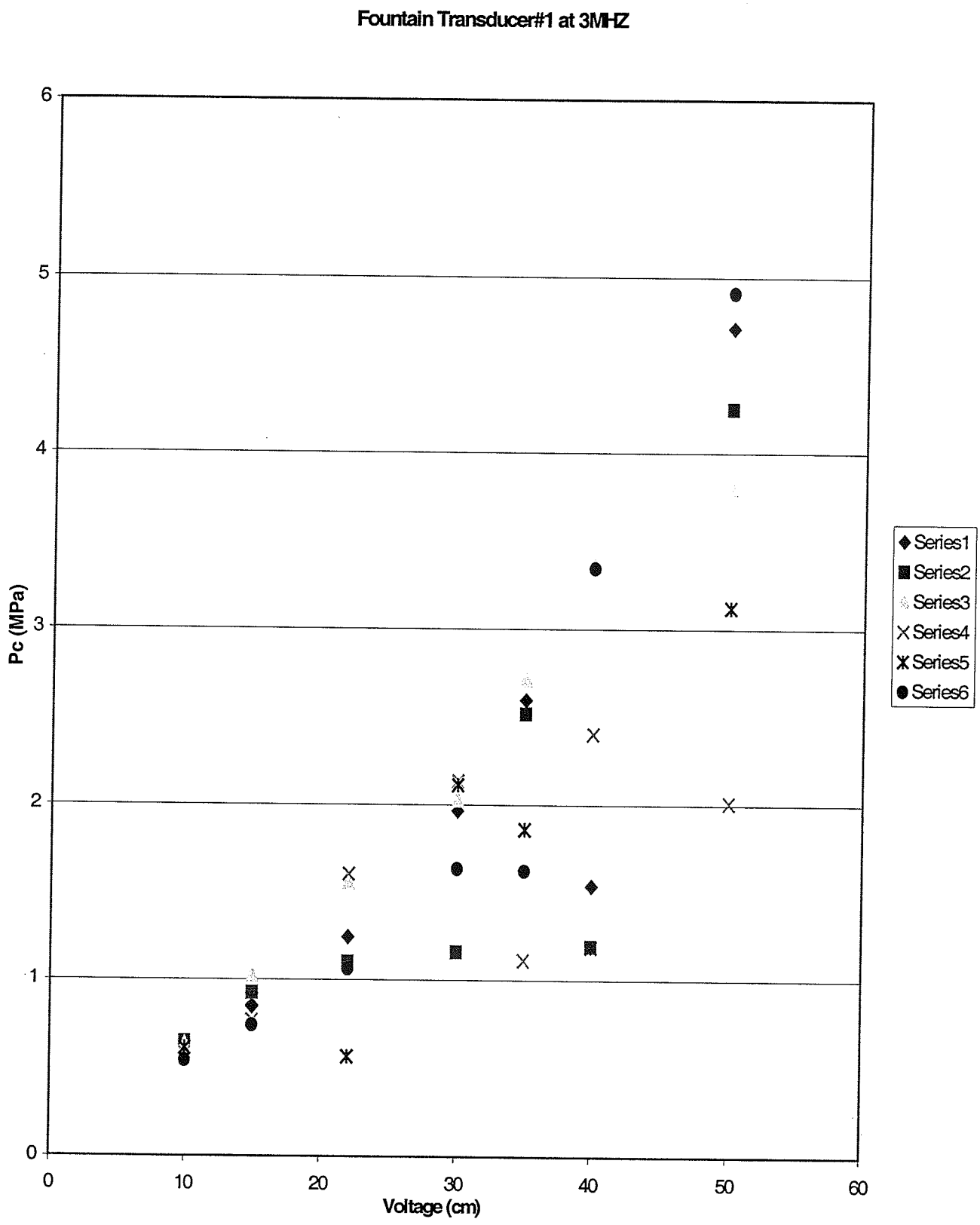

Figure A.1 Distribution of the compressional pressure from the results of the calibrations for FT#1 at 3 MHz.

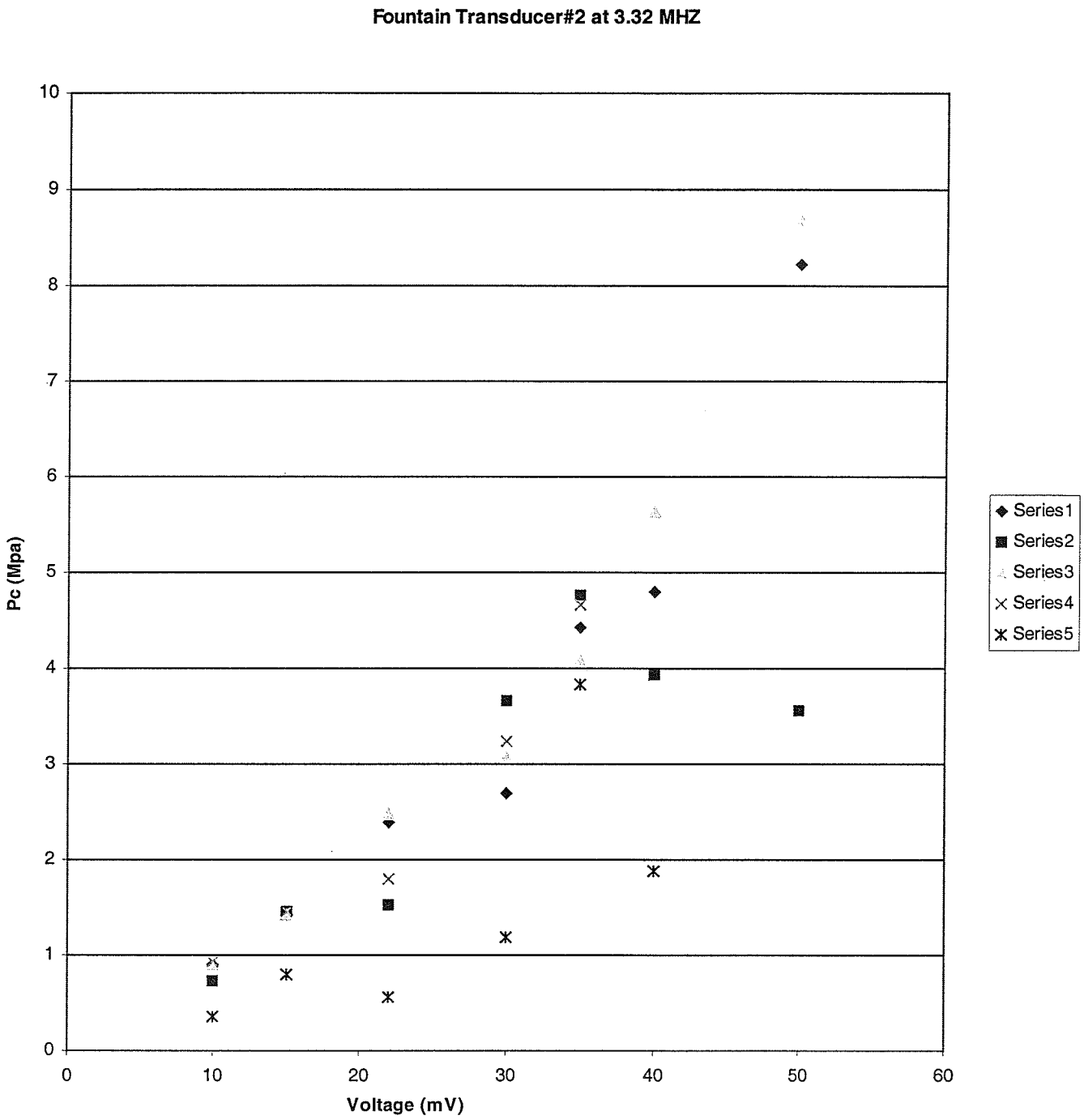

Figure A.2 Distribution of compressional pressure for FT#2 at 3.32 MHz

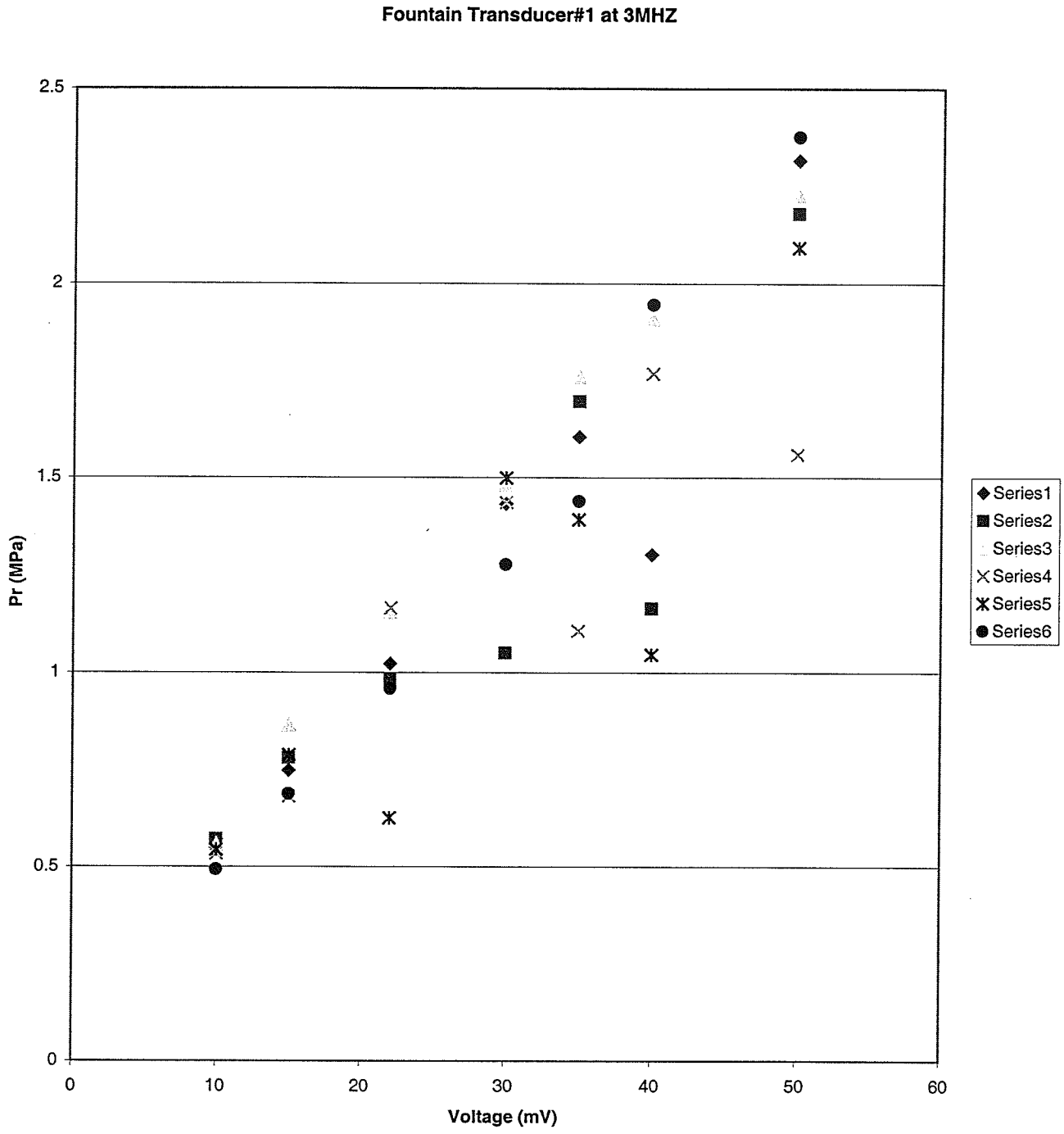

Figure A.3 Distribution of rarefactional pressure from the calibration results for FT#1 at 3MHz.

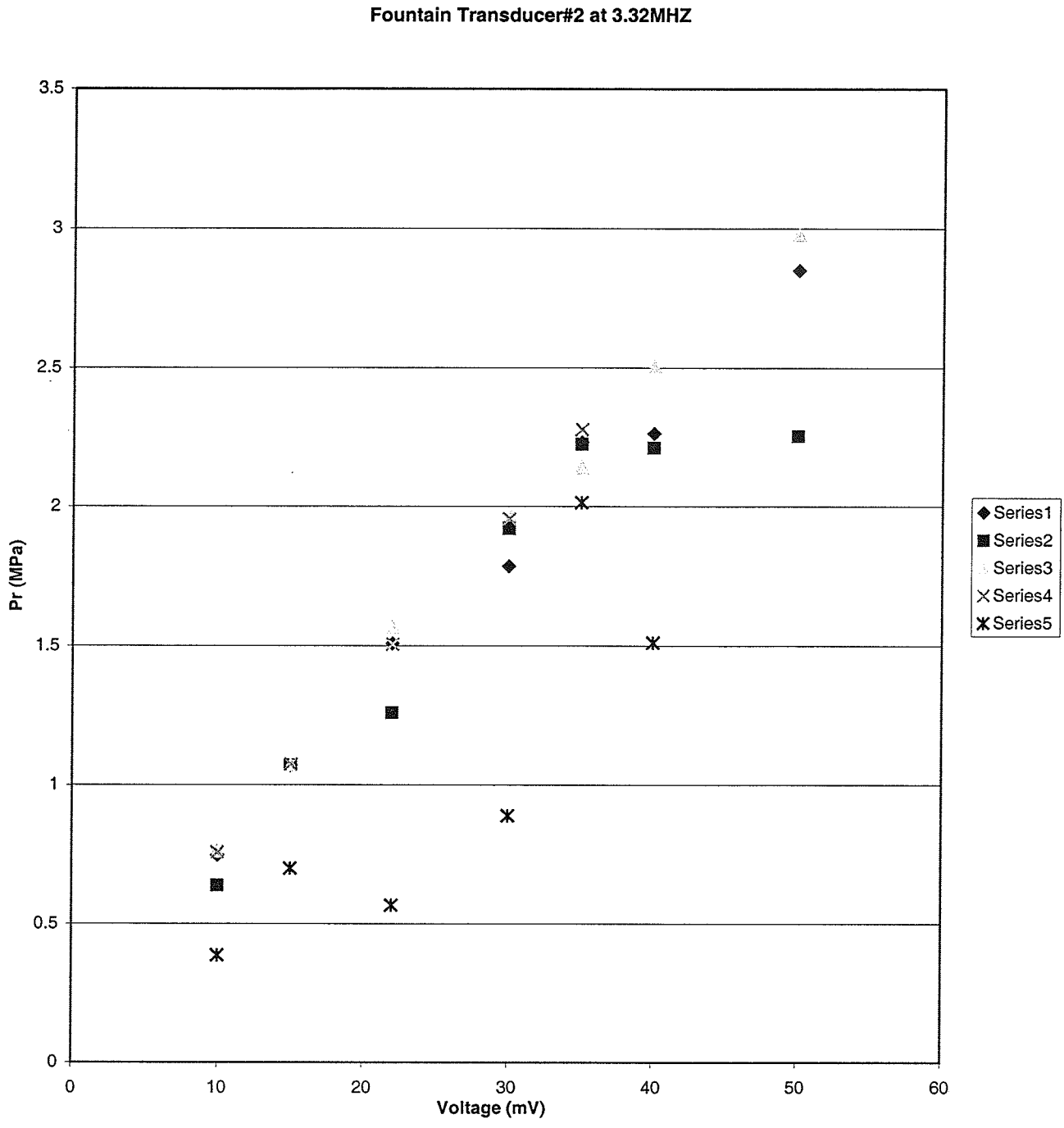

Figure A.4 Distribution of rarefactional pressure from the calibration results for FT#2 at 3.32MHz.

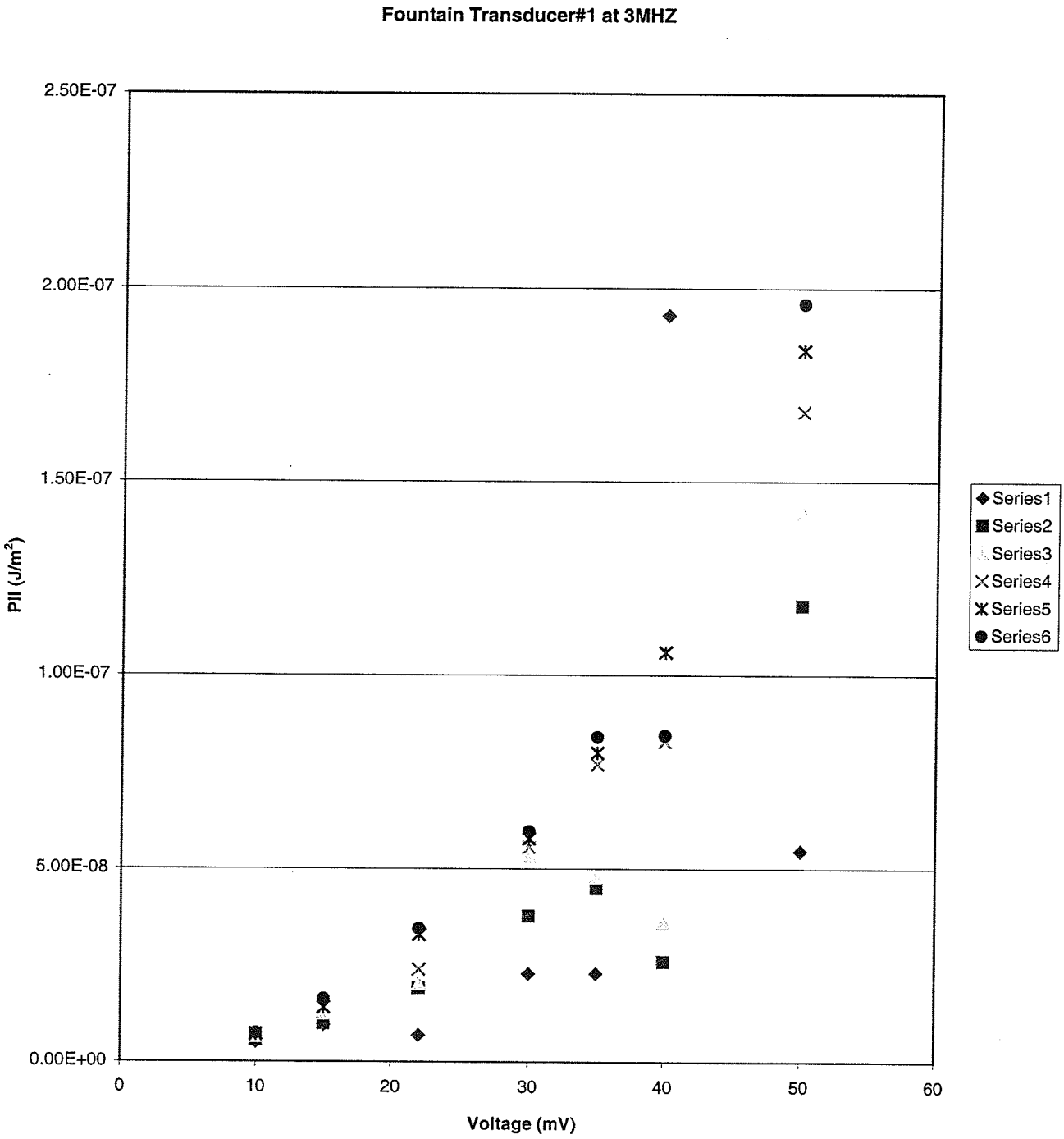

Figure A.5 Distribution of the maximum pulse intensity integral values for FT#1 at 3MHz.

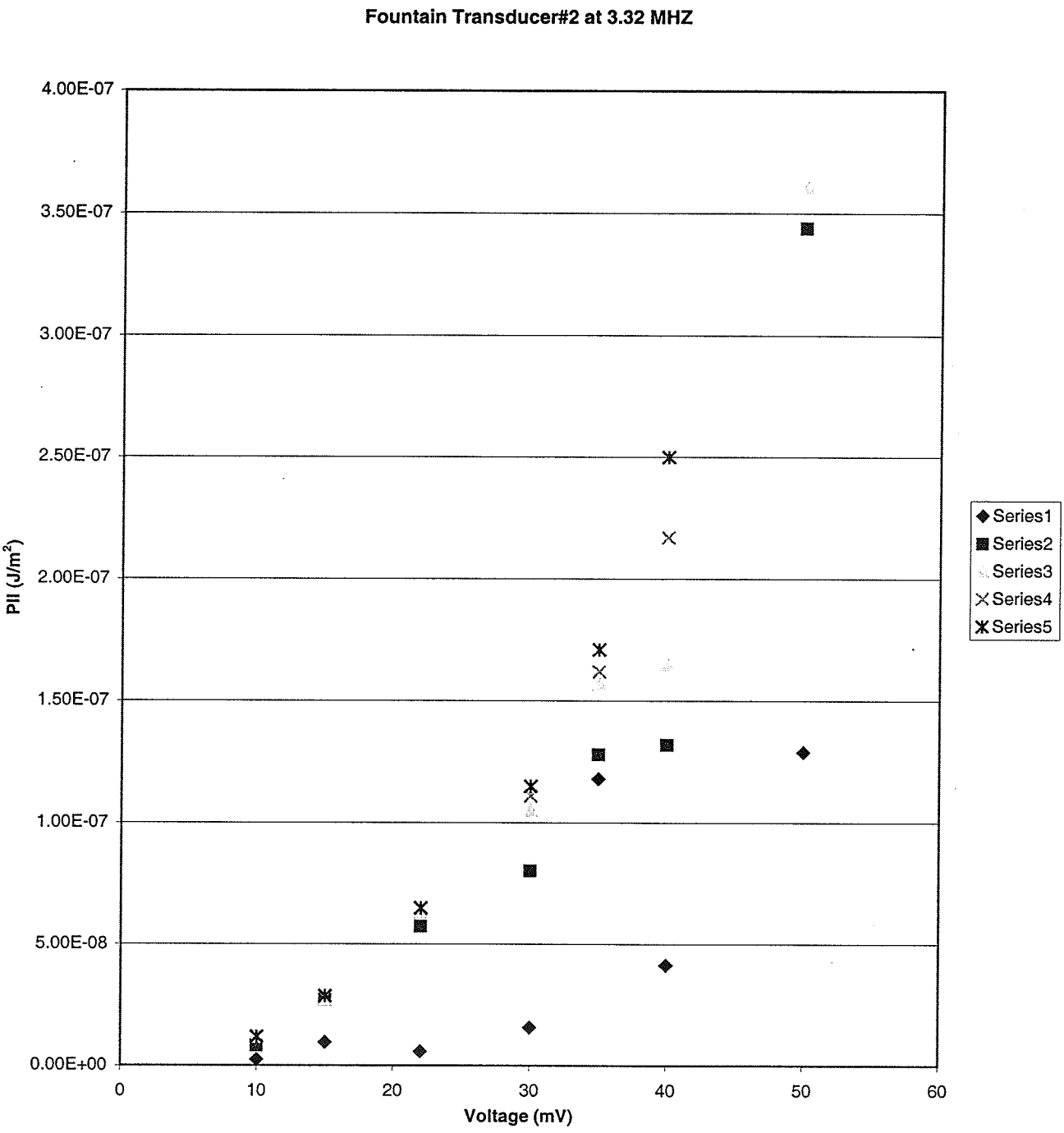

Figure A.6 Distribution of maximum PII values at each of the calibrated voltage value for FT#2 at 3.32MHz.

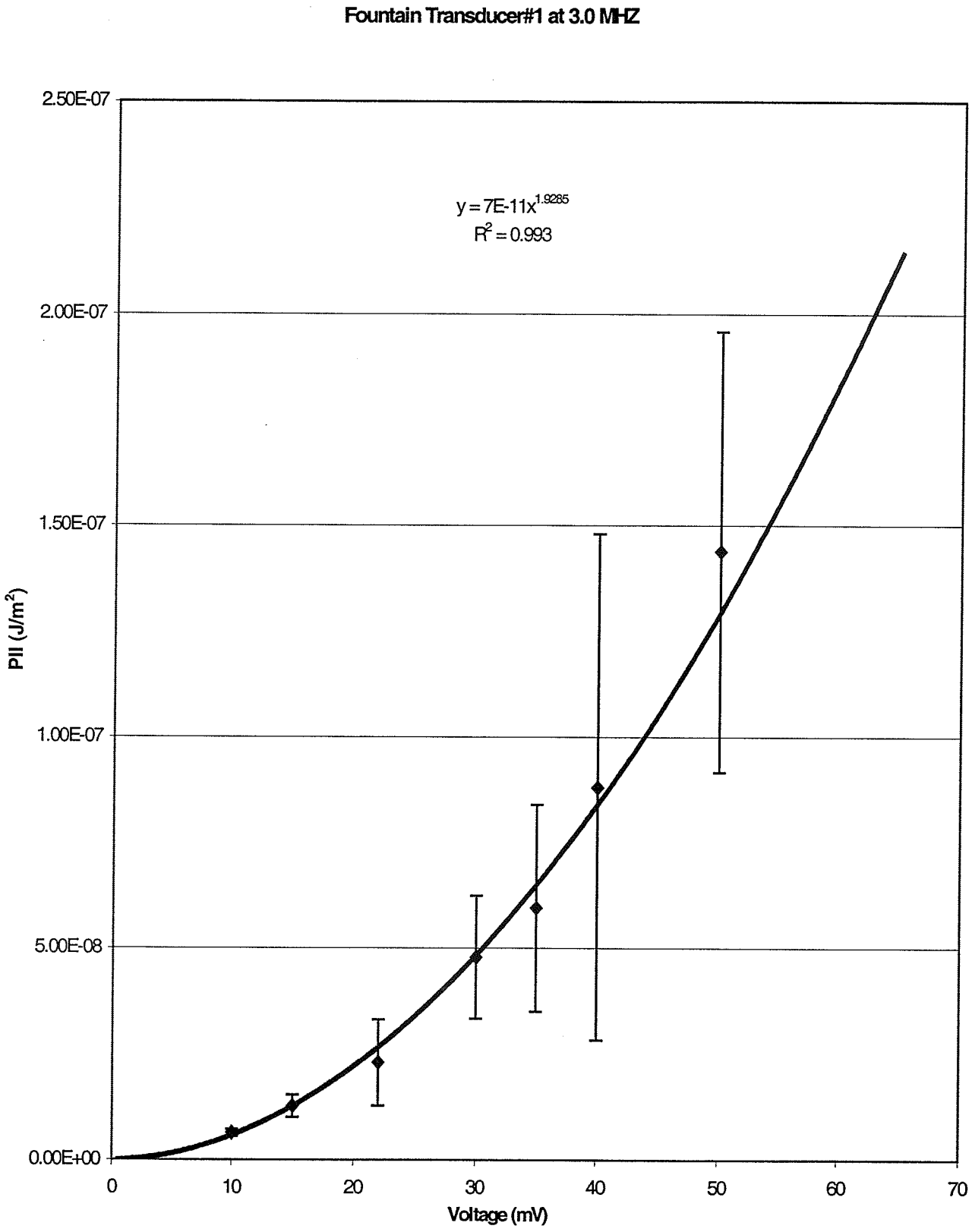

Figure A.7 Indicates that PII increases with voltage and that the standard deviation is larger at higher voltage because of the nonlinear effect.

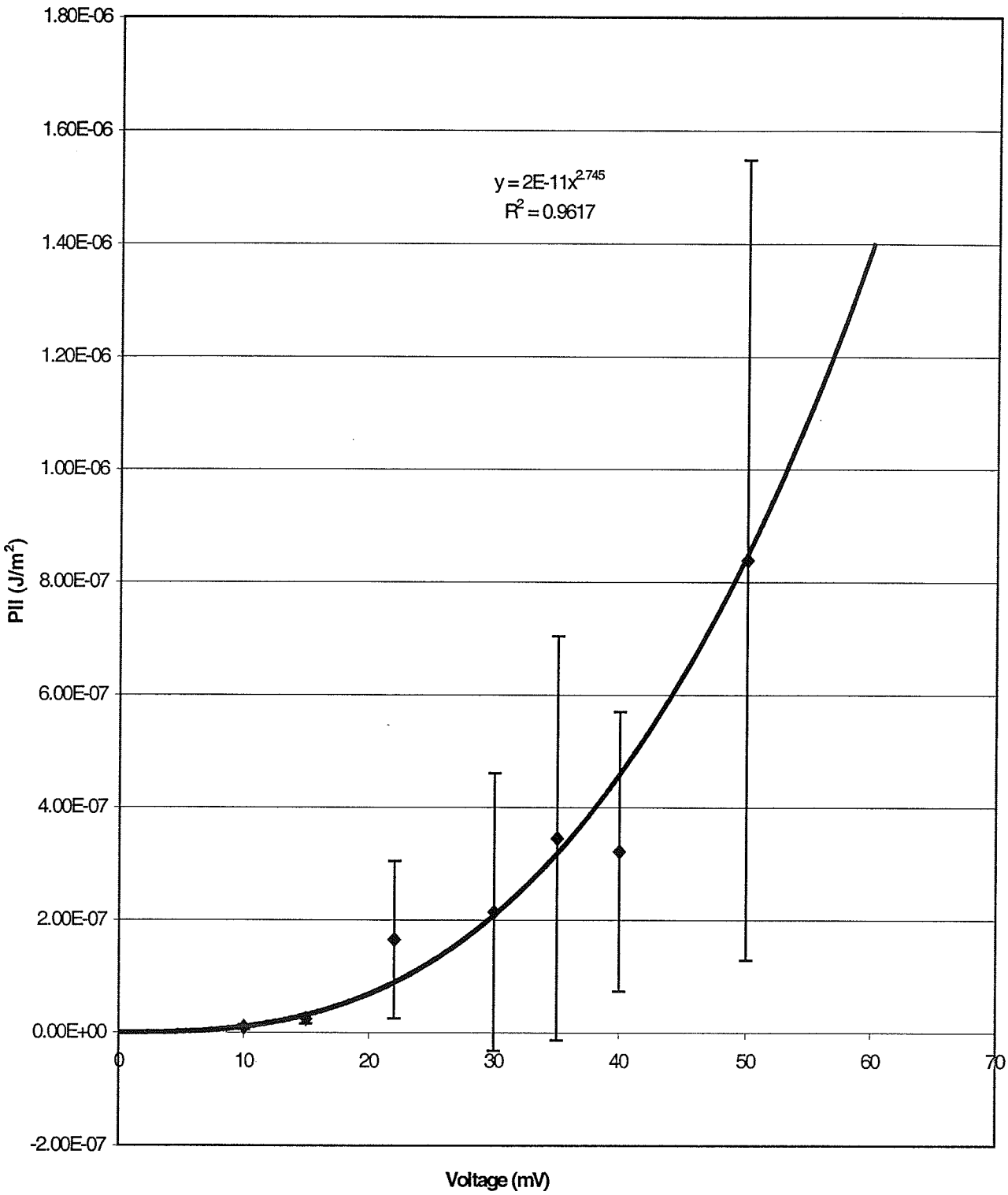

Figure A.8 Indicates that PII increases with voltage and that the standard deviation is larger at higher voltage because of the nonlinear effect.

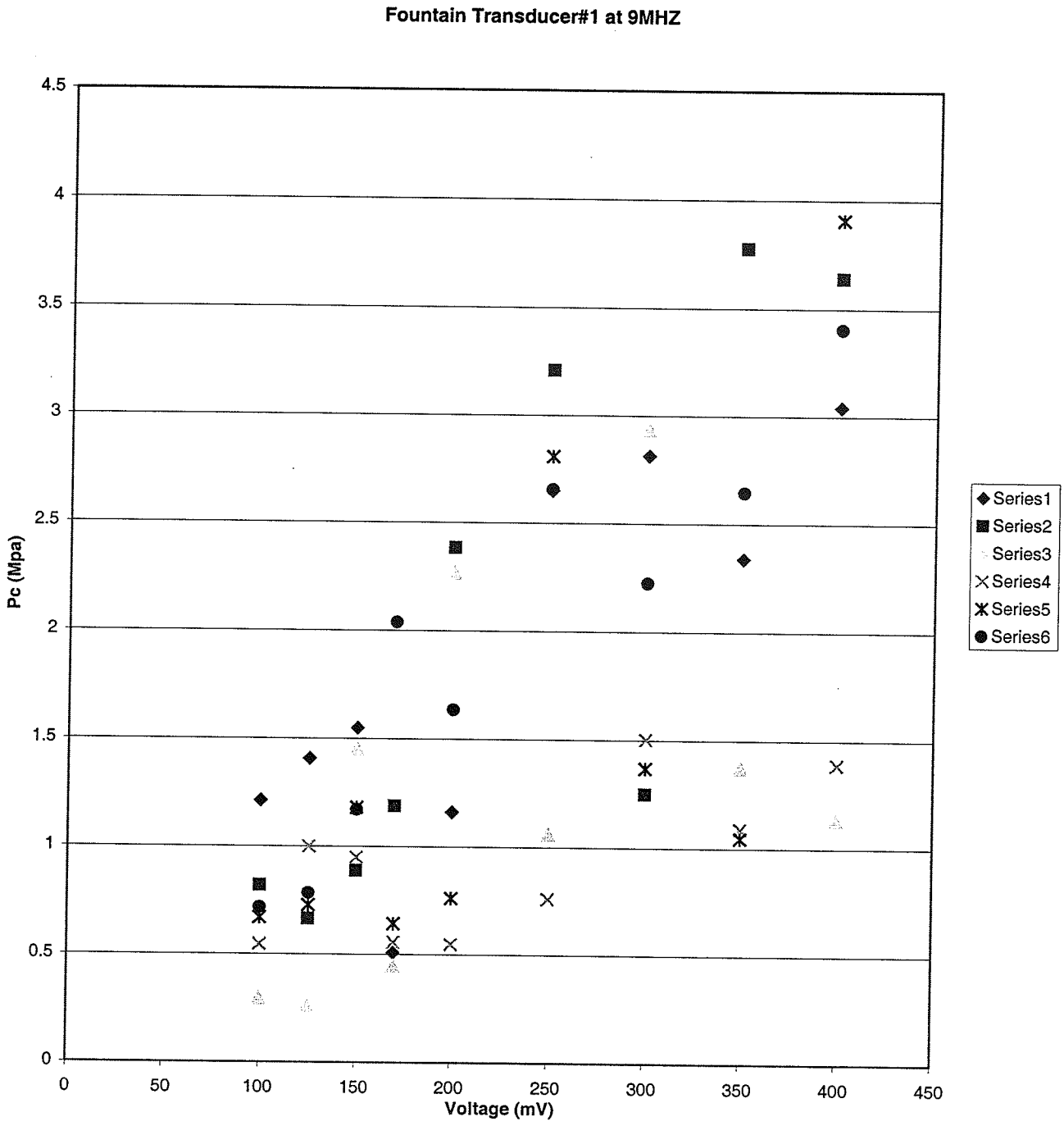

Figure A.9 Distribution of compressional pressure for FT#1 at 9MHz.

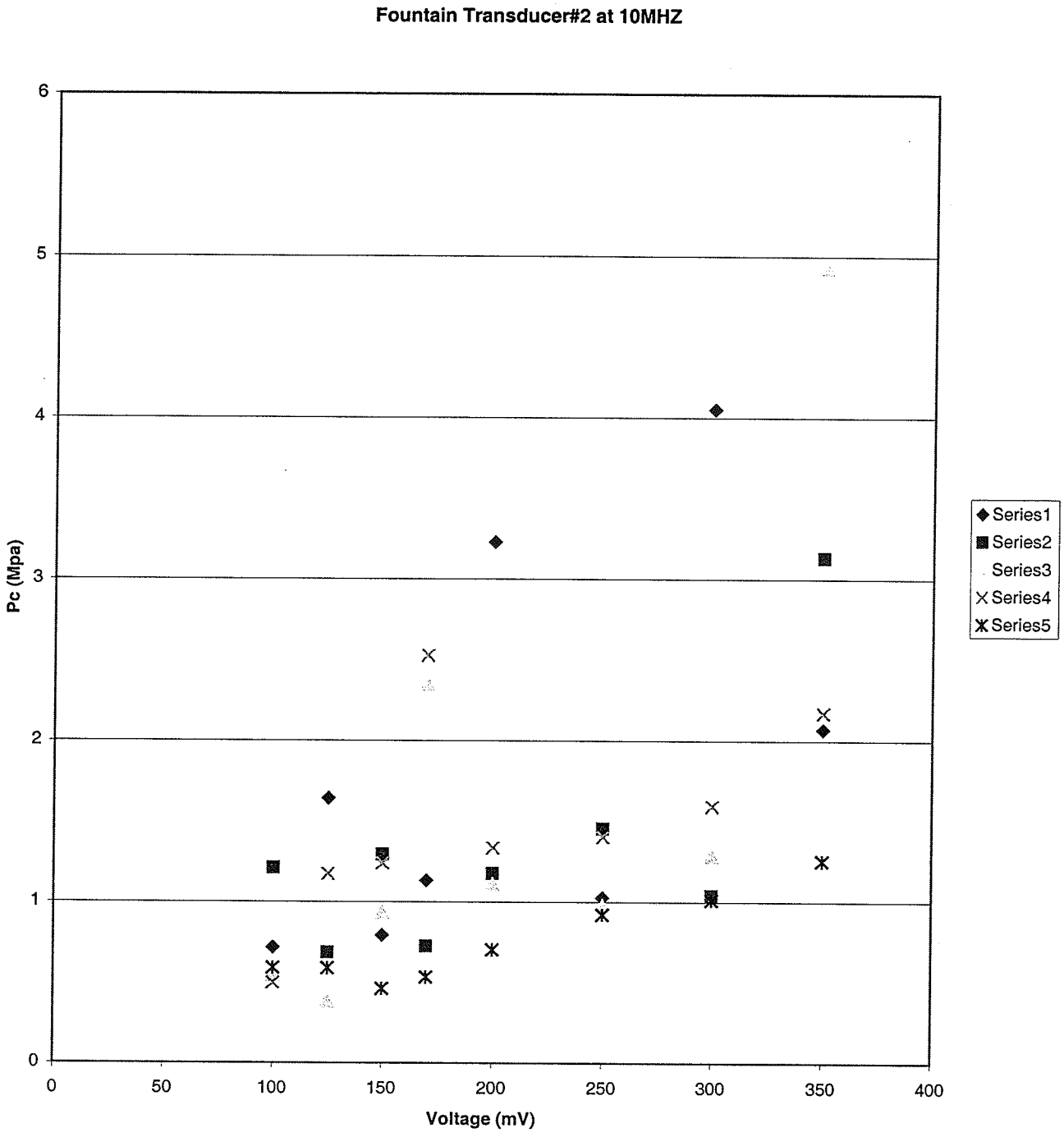

Figure A.10 Distribution of compressional pressure for FT#2 at 10MHz.

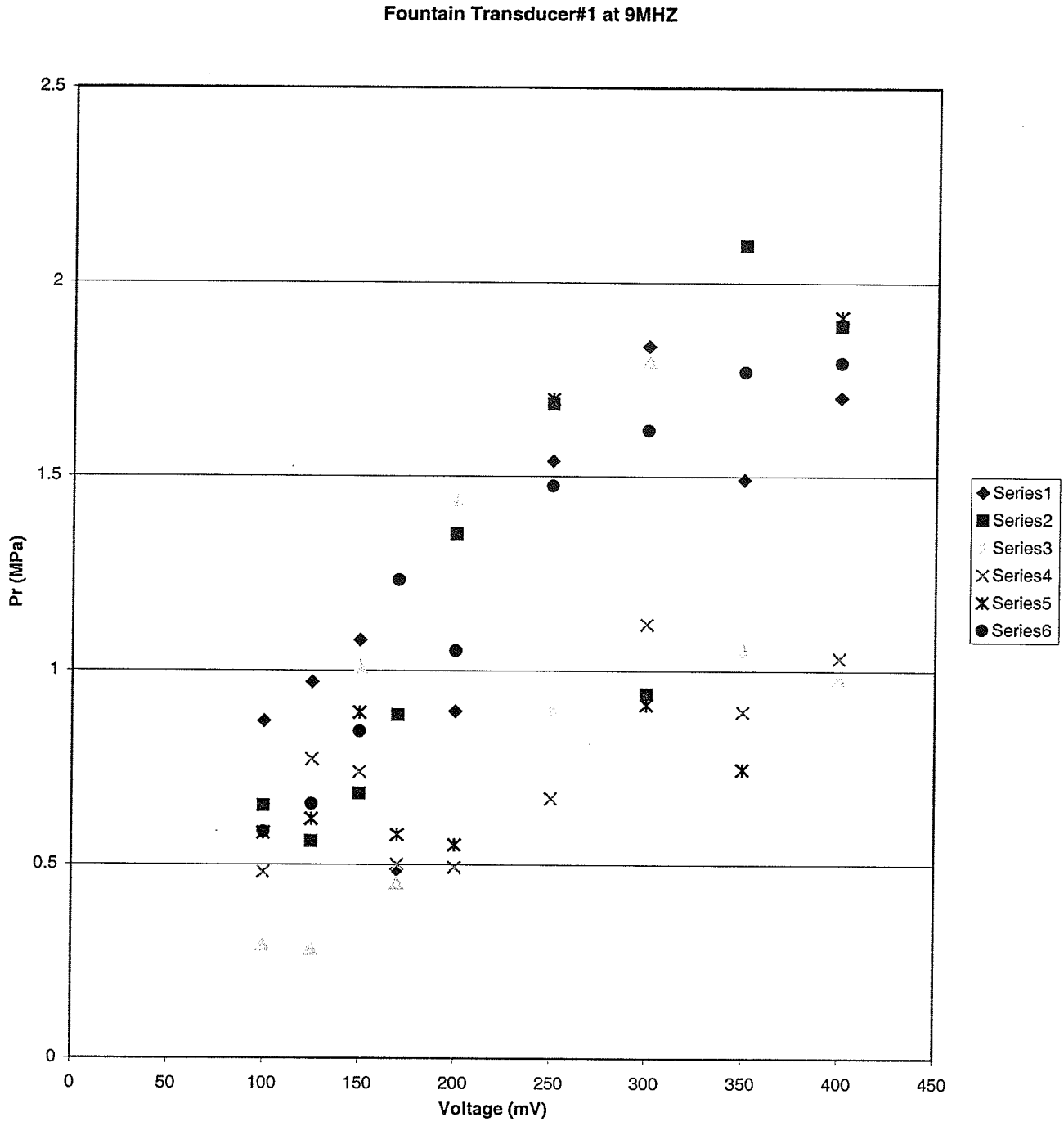

Figure A.11 Distribution of rarefactional pressure for FT#1 at 9MHz.

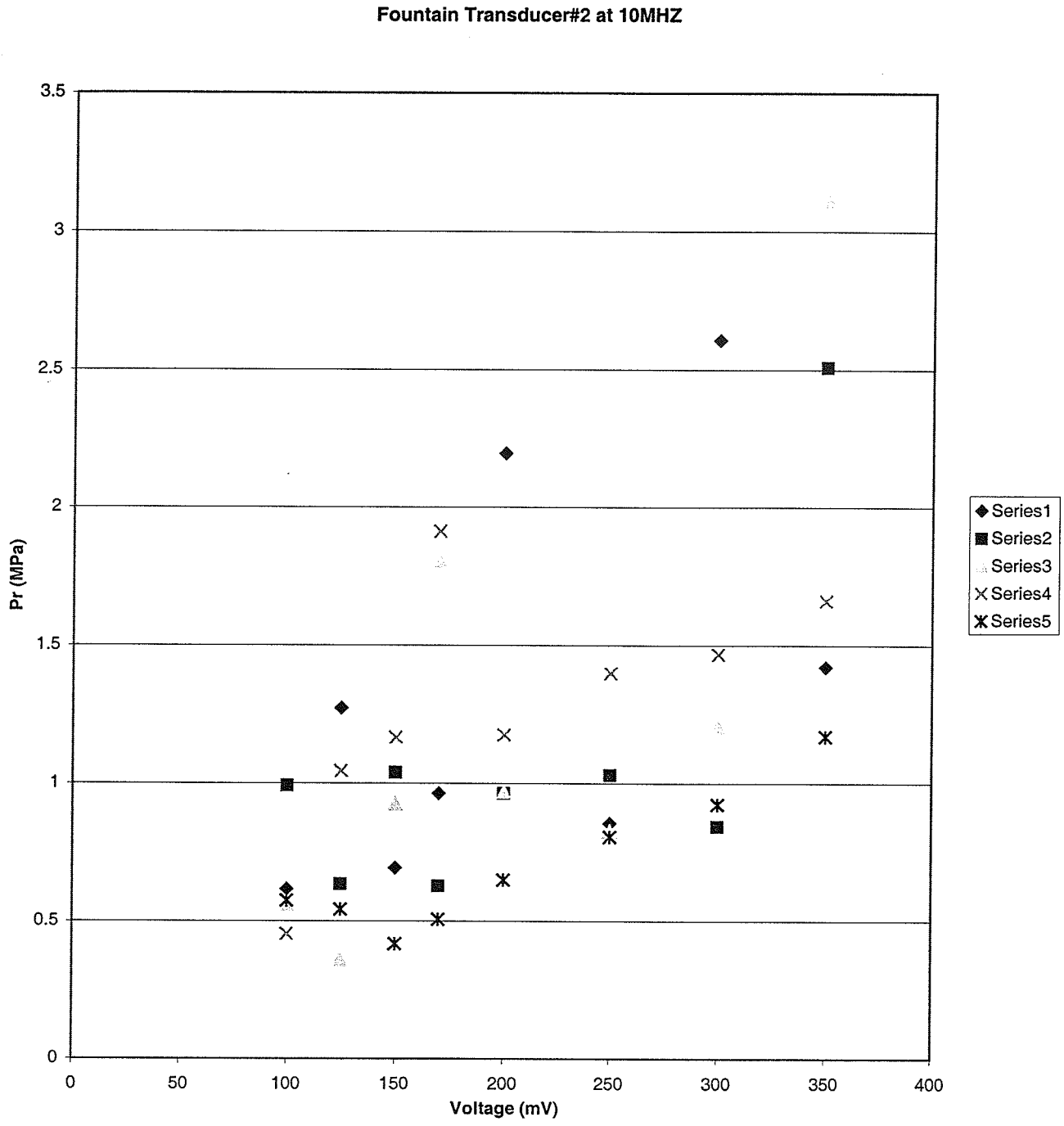

Figure A.12 Distribution of rarefactional pressure for FT#2 at 10MHz.

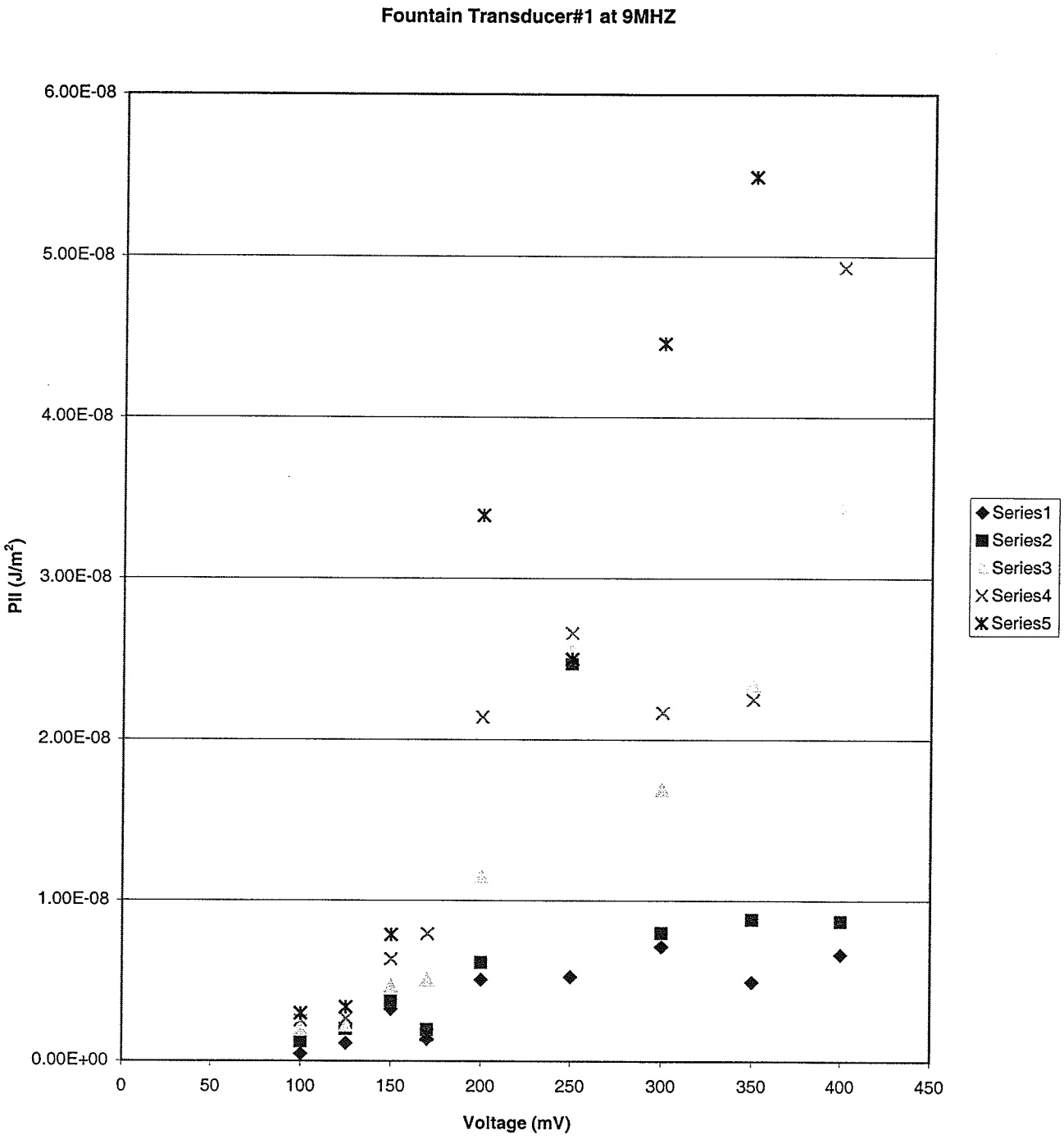

Figure A.13 Distribution of maximum PII values for FT#1 at 9MHz.

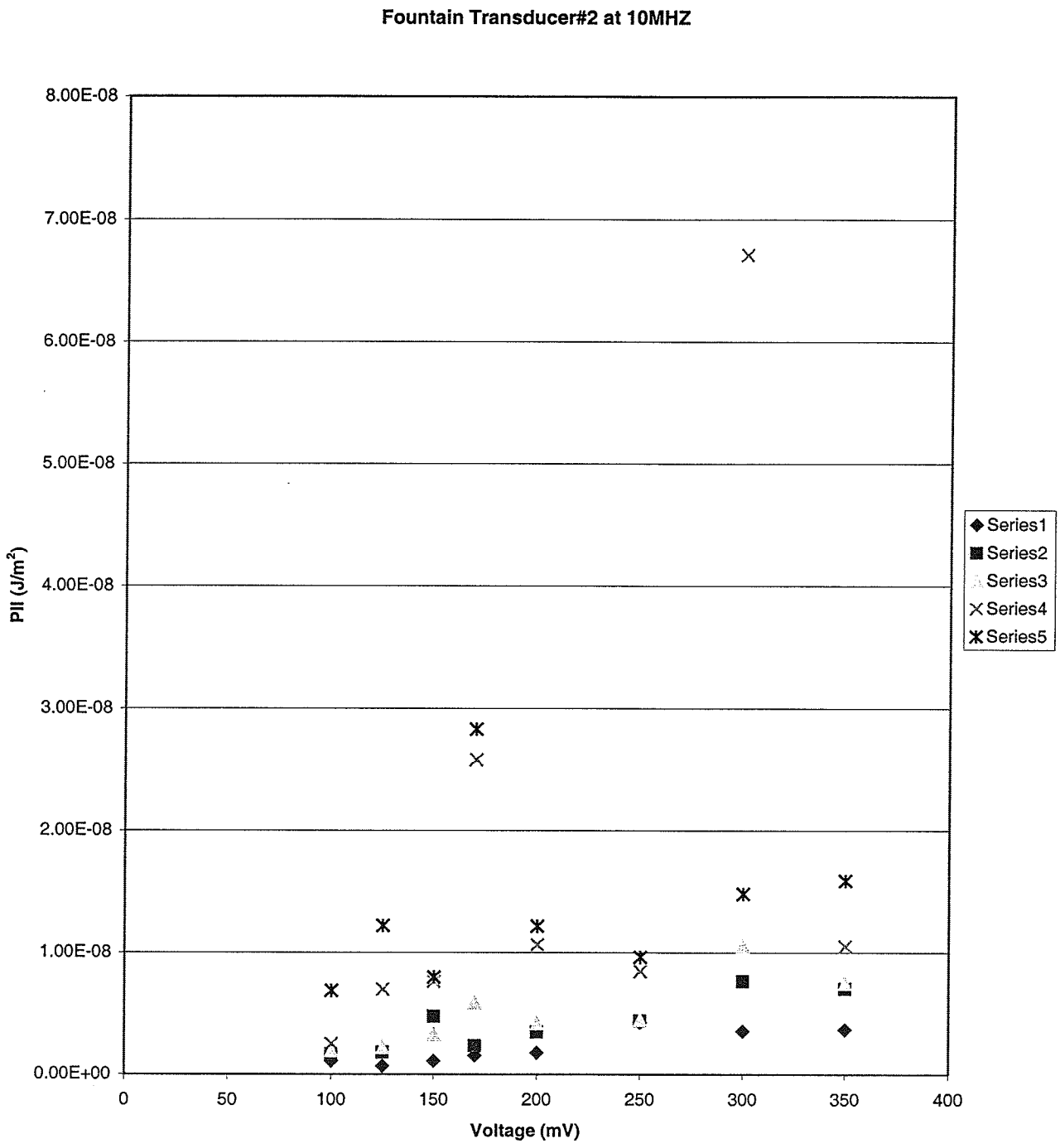

Figure A.14 Distribution of maximum PII values for FT#2 at 10MHz.

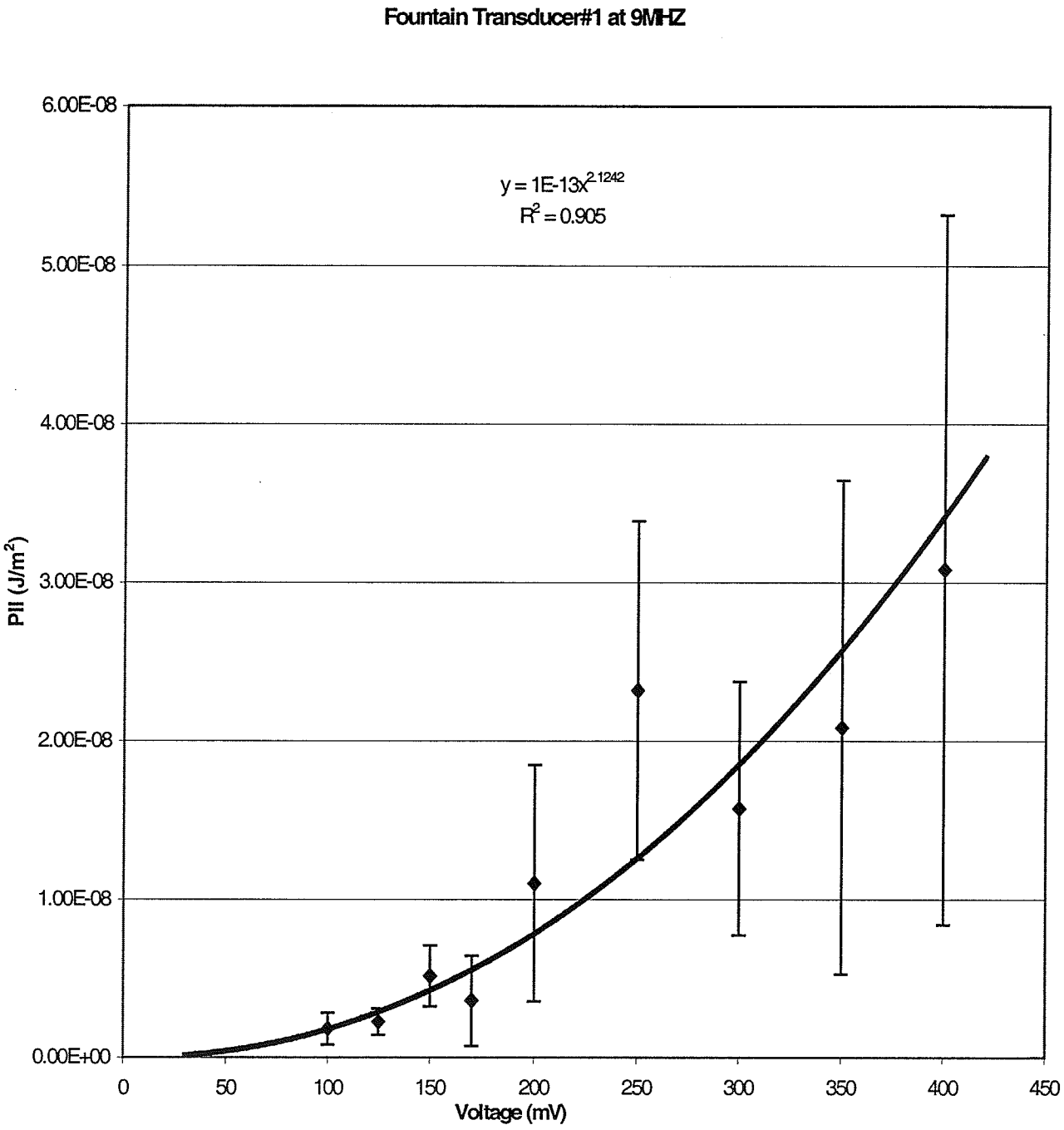

Figure A.15 Maximum PII value increases with increasing voltage. As the voltage increases the standard deviation of PII increases due to the non-linearity of the acoustic wave.

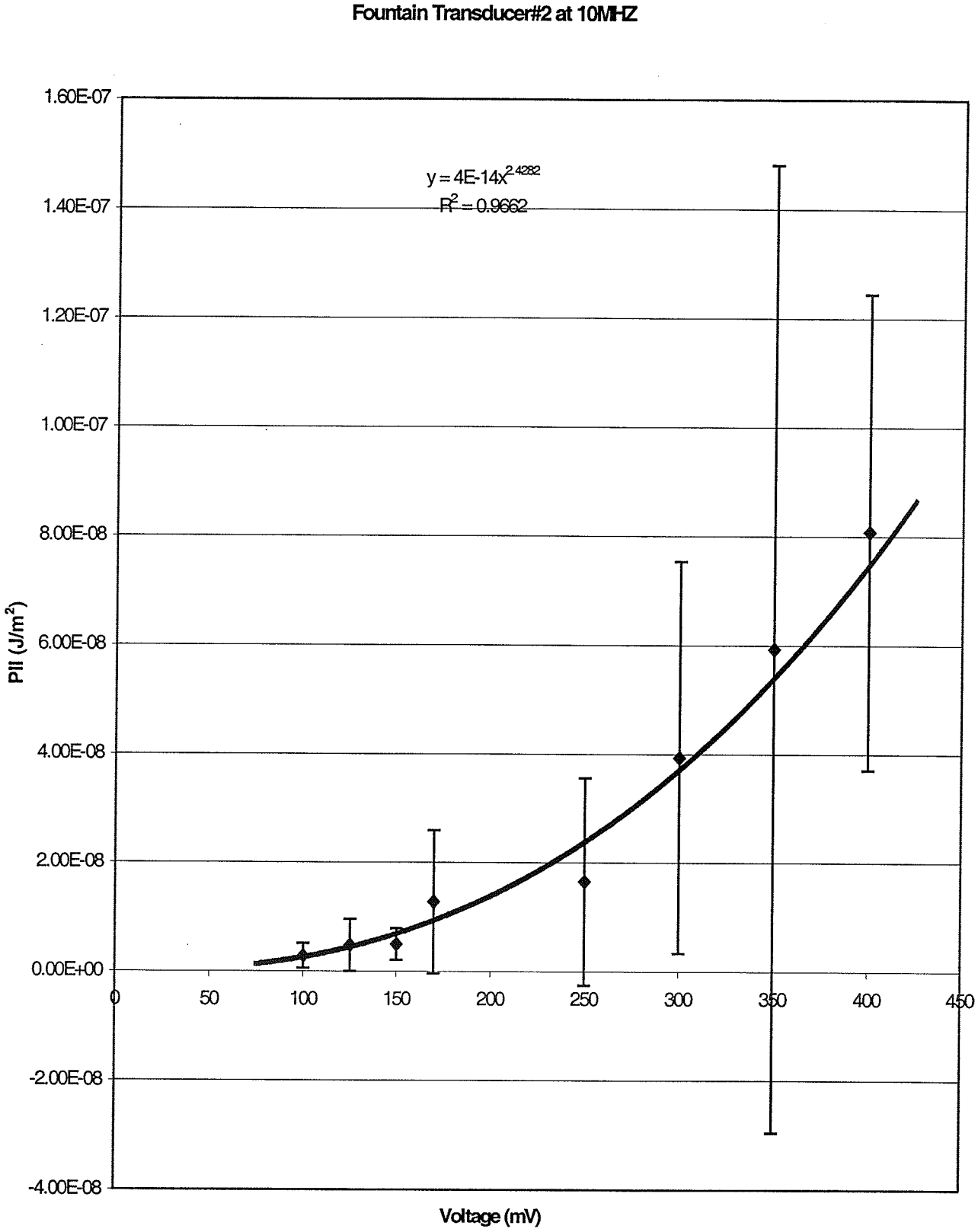

Figure A.16 Maximum PII values become unpredictable as the voltage value increases. This can be seen from the large standard deviations.